ISSN 0016-7029, Geochemistry International, 2007, Vol. 45, No. 5, pp. 428–450. © Pleiades Publishing, Ltd., 2007.
Original Russian Text © R.I. Mil'kevich, T.A. Myskova, V.A. Glebovitsky, A.B. L'vov, N.G. Berezhnaya, 2007, published in Geokhimiya, 2007, No. 5, pp. 483–506.

Kalikorva Structure and Its Position in the System of the Northern Karelian Greenstone Belts: Geochemical and Geochronological Data

R. I. Mil'kevich, T. A. Myskova, V. A. Glebovitsky, A. B. L'vov, and N. G. Berezhnaya

Institute of Precambrian Geology and Geochronology, Russian Academy of Sciences, nab. Makarova 2, St. Petersburg, 199034 Russia
e-mail: Lvov@TM13667.spb.edu

Received May 20, 2005

Abstract—New geochemical data on volcanic rocks and the first U–Pb zircon ages for the Kalikorva structure made it possible to determine the time and conditions of their formation and constrain geodynamic models. The lower sequences of the Kalikorva structure is dominated by metatholeiites with high MgO, Cr, and Ni contents, high *Mg*#, and REE distribution patterns close to the mantle level. They contain rare komatiite interlayers and lenses of pyroxenites and peridotites and can be considered as products of the deep melting of mantle material. At the same time, the tholeiitic metabasalts bear island-arc signatures and are intercalated with metagraywackes and metadacites (adakites). This rock association could be formed under spreading conditions at the beginning of an island-arc regime. The upper sequence is dominated by metagraywackes and contains diverse rocks with both MORB (tholeiitic and komatiitic basalts) and island-arc (calc-alkaline andesite and dacites, subalkaline basalts, and picritic basalts) affinity, which is typical of back-arc basins. The U–Pb dating of zircons from the metadacites and detrital zircons from the metagraywackes of the Kalikorva structure yielded similar ages of 2785 ± 13 and 2766 ± 21 Ma, respectively. They coincide with the age of the late volcanic complex of the Hisovaara Group of the Hisovaara structure (2780 Ma). Both complexes include island-arc associations with subduction signatures and contain adakites, Nb–Ti basalts, and basaltic andesites. The metagraywackes and metadacites of the Chupa sequence of the Belomorian mobile belt are older than the similar rocks of the Kalikorva complex and have an age of 2870 ± 30 Ma. Ages of 2735 ± 20 Ma and 2720 ± 4 Ma were previously obtained for the metaandesites of the Kichany volcanogenic complex, which could be an even younger volcanic arc.

DOI: 10.1134/S0016702907050023

INTRODUCTION

Recent studies [1–5] in the eastern Baltic Shield revealed a lateral series of sequentially formed nappes at the boundary between the Karelian craton and the Belomorian mobile belt. These nappes reflect the Late Archean evolution from subduction to collisional stages. They have the following structure (from east to west): (1) mafic zones representing fragments of the protooceanic crust with ophiolite-type stratigraphy within the Khetolambina nappe; (2) paragneisses, mainly graywackes, within the Chupa nappe (accretionary prism); and (3) system of greenstone belts of northern Karelia within the Kovdozero nappe composed mainly of calc-alkaline felsic and intermediate volcanic rocks (island arc at the margin of the Karelian craton).

The system of greenstone belts of northern Karelia consists of supracrustal structures exposed as a chain at the boundary between the Karelian craton and the Belomorian mobile belt (BMB). According to Kozhevnikov [6] and Slabunov [4], they are morphologically different fragments of a single volcanic belt, which reflect different stages of its evolution from young to mature island arcs.

The appearance of felsic and intermediate volcanics and some geochemical features are important arguments in favor of Late Archean subduction, and their ages define, therefore, the timing of subduction. However, this model is yet poorly constrained by geochemical and geochronological data, which are available only for a few individual structures [7, 8]. Therefore, an important task is thorough geological, geochronlogical, geochemical, and isotopic study of the fragments of supracrustal rocks and the analysis of their interaction. Detailed studies in some structures, for example, Hisovaara [9], revealed a complex evolution of island arc systems. The authors of these studies showed that this is an accretionary system consisting of at least two island arcs with ages of felsic and intermediate magmatism of 2.78–2.82 and 2.82–2.88 Ga.

This study focuses on the supracrustal rocks of the Kalikorva antiform structure located in the western part of Kovdozero Lake. The structure is composed of supracrustal rocks in the core and tonalitic gneisses at the limbs (Fig. 1). The lower part of the volcanic–sedimentary sequence is composed mainly of metabasalts, and the upper part is dominated by metagraywackes. The Kalikorva supracrustal complex was first recognized during geological mapping in 1951 by G.A. Porotova and K.P. Galetskaya. Based on the unusual trefoil shape of the structure, Gorlov [12] considered it as a synform located at the junction of three domes. However, recent detailed structural–geological studies [3, 10] suggested that this structure is a tectonic window composed of the rocks of the Chupa nappe. The problem was to determine the timing of formation of the tectonic nappe during subduction or collision between the island arc and the continental margin. An additional argument in favor of uniting the Kalikorva and Chupa complexes was the geochemical similarity of metasediments, which are represented by immature graywackes with a significant contribution of mafic material into the model source area and their similar Sm–Nd model ages of 2.8–2.9 Ga [10, 13]. However, some compositional features and the spatial position of these complexes cast some doubt on their correlation. The sections of the Chupa and Kalikorva complexes are widely spaced and have significantly different contents of volcanics rocks (5–10% in the former and up to 50% in the latter). The geochemistry of the graywackes points to independent source areas. There are also some differences between the compositions of volcanic rocks. However, the latter have been less studied than the graywackes. New geochemical data on the volcanic rocks and the first U–Pb zircon ages obtained for this area provided insight into the time and formation conditions and allowed us to refine geodynamic reconstructions.

GEOLOGY AND COMPOSITION OF THE KALIKORVA COMPLEX

Since the Kalikorva structure appeared to be formed by the deformation of a series of nappes, the observed sequence of supracrustal rocks is tectonostratigraphic and may not correspond to their primary sequence.

The lower sequence is composed of garnet and garnet–clinopyroxene amphibolites corresponding to tholeiitic basalts with rare interlayers of biotite–amphibole (occasionally, garnet-bearing) dacitic and andesitic gneisses and garnet–biotite (occasionally, kyanite-bearing) gneisses (metagraywackes). The amphibolites contain a few thin interflows similar in composition to komatiitic basalts and Fe–Ti tholeiites. Various gabbroids are common in the structure, especially in its western part. Some of them pertain to the drusite complex with an age of 2450 Ma and form small gabbronorite bodies. The large Kovdozero intrusion of the same age is located northwest of the area.

The upper sequence is dominated by garnet–biotite, occasionally, kyanite-bearing gneisses (metagraywackes) and thin alternation of rocks of different composition (Fig. 2): clinopyroxene–garnet–plagioclase amphibolites (metatholeiites) with thin (from a few cm to 1 m) layers of komatiitic metabasalts, amphibole–biotite–plagioclase (with garnet and epidote) schists (subalkaline basaltic andesites), biotite–amphibole–plagioclase (with garnet and clinopyroxene) amphibolites (subalkaline and picritic basalts), biotite–amphibole (occasionally with garnet) plagiogneisses (metadacite–adakite), and biotite–garnet–kyanite gneisses (HREE-enriched dacites). Metatholeiites and metadacites also occur as individual interlayers among metagraywackes. All the rocks were affected by amphibolite-facies metamorphism and strong schistosity, which obliterated their primary structures and contacts. Therefore, it is unclear whether they were formed as extrusive rocks or whether some of them belong to dike swarms.

GEOCHEMISTRY

The chemical compositions of the volcanic rocks are shown in Fig. 3. Tables 1–2 give the representative compositions of major rock types.

Lower sequence. Most of the amphiboliltes chemically correspond to Mg tholeiitic basalts and are close to tholeiite I [16]. They are low-Ti and moderately aluminous. In the $MgO–TiO_2$ diagram (Fig. 4a), they plot in the tholeiite series field near the boundary with the komatiite series. The trace element ratios (average of 45 analyses) Ti/Zr = 102.43, Zr/Y = 2.48, and Al_2O_3/TiO_2 = 14.83 are close to the chondritic values. The high Cr and Ni contents suggest high temperatures of primary melts. In the Zr/Y–Nb/Y diagram (Fig. 4b), they fall within the field of oceanic plateau basalts. Rocks corresponding to komatiitic basalts and Fe tholeiitic basalts are much less common.

The komatiitic metabasalts (samples 450/1 and 432/3, Table 1) contain up to 16% MgO and have $Mg\#$ = 67–71, low Al_2O_3, and high Cr contents. The Fe-rich amphibolites (typically, amphibole–plagioclase rocks) occur as thin intercalations (sample 449/3) and subconcordant metagabbroid bodies (samples 1228b and 1679/3) among amphibolites. Compared with the Mg metabasalts, they are enriched in Fe_2O_3, TiO_2, V, Cr, and REE but depleted in Cr and Ni. Similar rocks were reported from the Hisovaara structure of the Tikshozero greenstone belts [9] and some greenstone belts of the Superior Province [19]. However, it should be taken into account that similar geochemical characteristics are typical of Fe tholeiites with an age of 2100 Ma [20]. Therefore, isotope–geochemical studies are required to reliably determine the nature of these rocks. Intrusive rocks are also represented by sporadic bodies of metaperidotites and Mg gabbroids. The metaperidotites contain up to 43.8% SiO_2, up to 35% MgO, 4778 ppm Cr, and 1180 ppm Ni and are presumably cumulates.

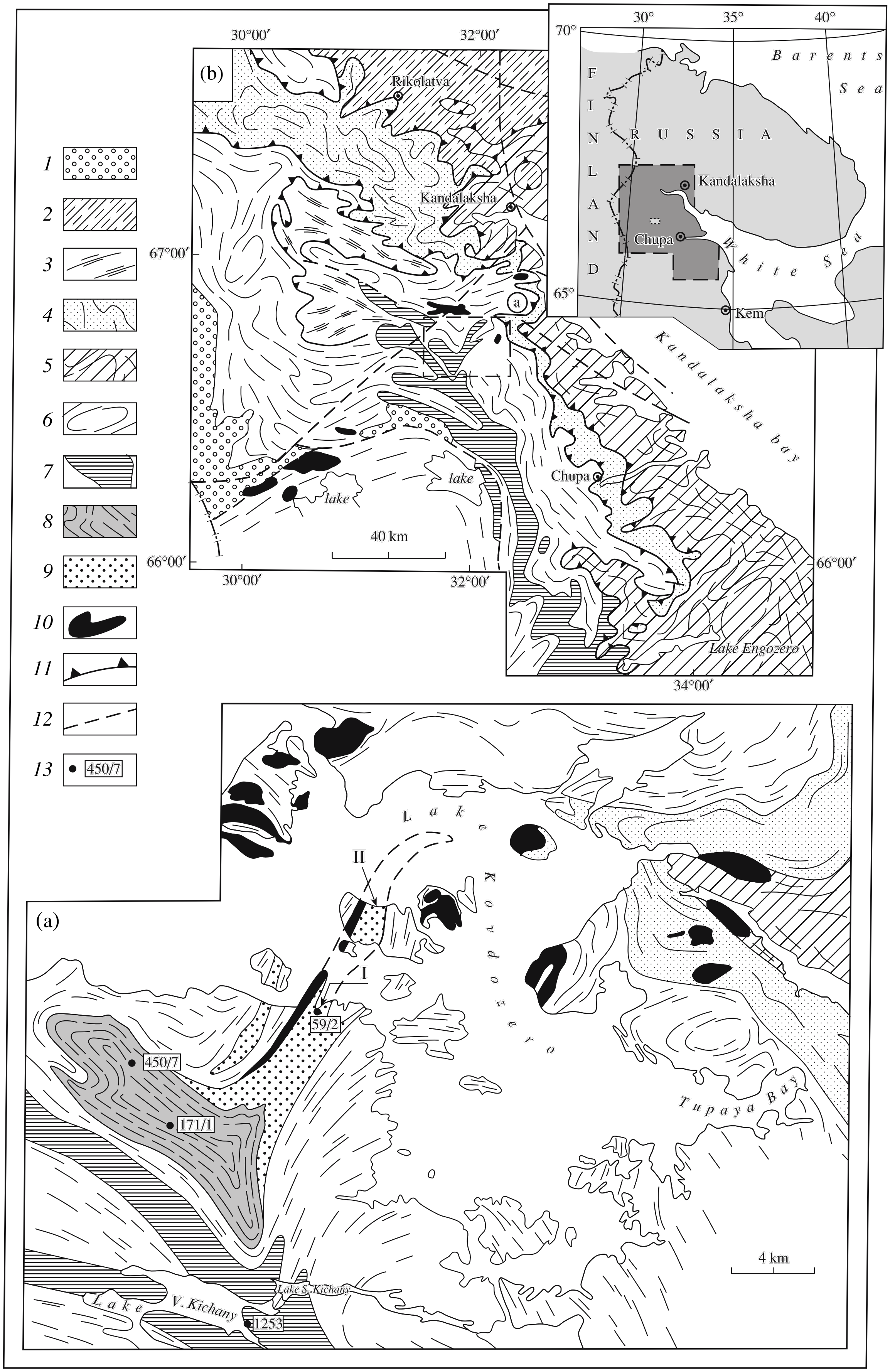
(b)
(a)
30°00′
32°00′
34°00′
67°00′
66°00′
Rikolatva
Kandalaksha
Chupa
lake
40 km
Kandalaksha bay
Lake Engozero
70°
65°
30°
35°
40°
Barents Sea
FINLAND
RUSSIA
White Sea
Kem
1
2
3
4
5
6
7
8
9
10
11
12
13
450/7
Lake Kovdozero
II
I
59/2
171/1
Tupaya Bay
4 km
Lake S. Kichany
Lake V. Kichany
1253

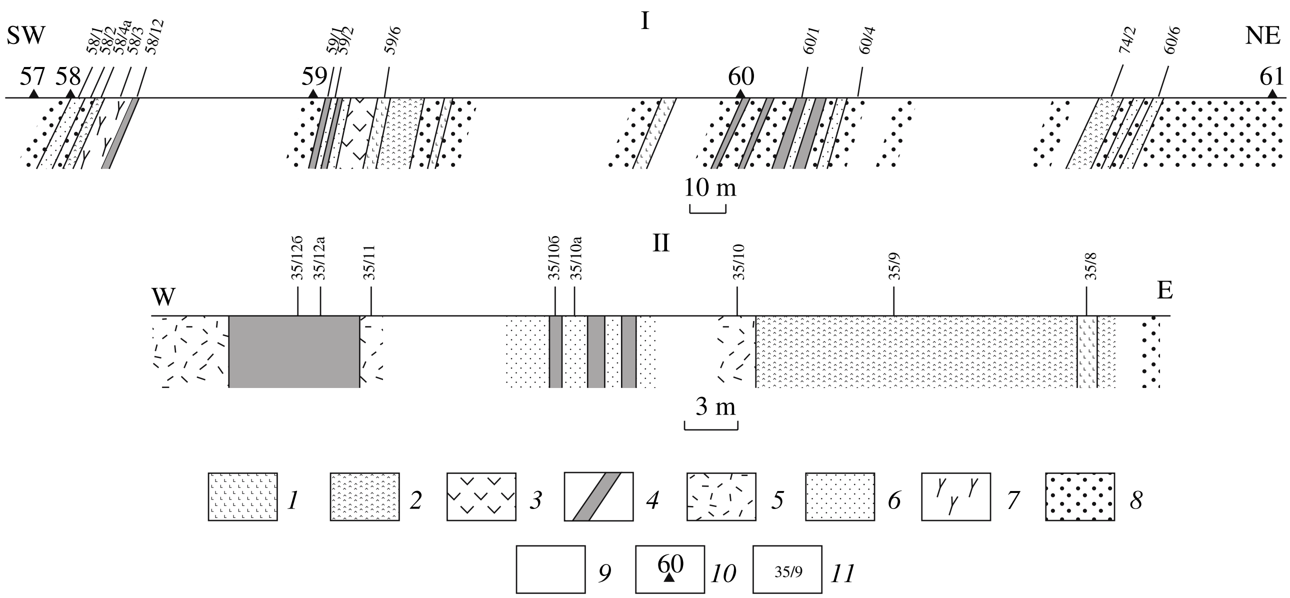

Fig. 2. Sections of the upper sequence in the areas of thin alternation of rocks. Roman numerals refer to the position of the sections in Fig. 1. (*1*) Komatiitic metabasalt, (*2*) magnesian tholeiitic metabasalt, (*3*) Fe-tholeiitic metabasalt, (*4*) subalkaline metabasalt and metapicritic basalt, (*5*) subalkaline metabasaltic andesites, (*6*) metadacite (adakite), (*7*) HREE-enriched metadacite, (*8*) metagraywacke, (*9*) no exposures, (*10*) outcrop number, and (*11*) sample number.

The Mg gabbroids (sample 1209b, Table 1) are high in MgO, Al_2O_3, Cr, Ni, and V and low in Zr contents. Similar to the tholeiites, they have almost chondritic Ti/Zr and Zr/Y values. In the Zr–Y diagram (Fig. 4c), they form a single evolution trend together with the metabasalts, which suggests their comagmatic origin.

However, the metabasalts are different in terms of REE distribution patterns. Figure 5a shows a geochemical group of weakly LREE depleted rocks with a minor Eu anomaly suggesting *Pl* fractionation during magma differentiation in an intermediate magma chamber or Eu mobility. The REE content is ten times chondrite with $(La/Yb)_N$ = 0.57–0.87. Sample 43 from the upper part of the section also belongs to this group.

Figure 5c shows tholeiites with unfractionated, $(La/Yb)_N$ = 0.89–0.97, but higher REE contents. The compositions of the adjacent layers of Fe-rich tholeiites are also plotted in this diagram. They are enriched in REE; samples 1679/1 and 1679/3 have parallel distribution patterns (probably indicating a common source), whereas sample 449/3 is enriched in LREE compared to tholeiites (sample 449/2) and has fractionated patterns (which may indicate a different source).

Figure 5e illustrates compositional variations within a single exposure of an 8-m-thick section. Metatholeiites are weakly fractionated, $(La/Yb)_N$ = 1.21–1.33. The only analyzed sample of komatiitic metabasalt from the upper part of the section appeared to be LREE enriched.

The primitive mantle-normalized trace element patterns show a negative anomaly of Ta relative to La (Nb and Th contents are below the analytical sensitivity). There are also a weak negative Ti anomaly and very small positive or negative Hf anomalies. These variations presumably indicate a contribution of subduction processes to the composition of the source.

The metadacites have high contents of Al_2O_3, Sr, and Ba; low Nb, Y, and Tb; high Sr/Y and La/Sm ratios; and no Eu anomaly. They are similar to adakites produced by the partial melting of a hot oceanic slab at high *T* and *P* [22, 23]. The adakites of the region show elevated Cr contents; steep REE distribution patterns (Fig. 6) with $(La/Yb)_N$ = 18.74–28.66; distinct negative

Fig. 1. (a) Geological sketch map of the Kalikorva area and (b) its position in the structure of the Belomorian mobile belt (modified after [10] and [11]). (*1*) Early Proterozoic troughs; (*2*) Svecofennian Rikolatva nappe; (*3–5*) Late Archean (Belomorian) allochthon: (*3*) Orijarvi nappe, tonalites, (*4*) Chupa nappe, aluminous gneisses (mainly metagraywackes) injected by tonalites, (*5*) Khetolambina nappe, tonalites with mafic–ultramafic bands; (*6–9*) Kovdozero Nappe: (*6*) tonalite-dominated infracrustal complex; (*7–9*) Tikshozero greenstone belt: (*7*) undifferentiated infracrustal complex, (*8*) mainly tholeiitic metabasalts, (*9*) mainly metagraywackes; (*10*) Late Proterozoic gabbronorite–lherzolite complex; (*11*) fault plane separating nappes; (*12*) fault; and (*13*) sampling site and number of a geochronological sample. Roman numerals denote the position of sections presented in Fig. 2.

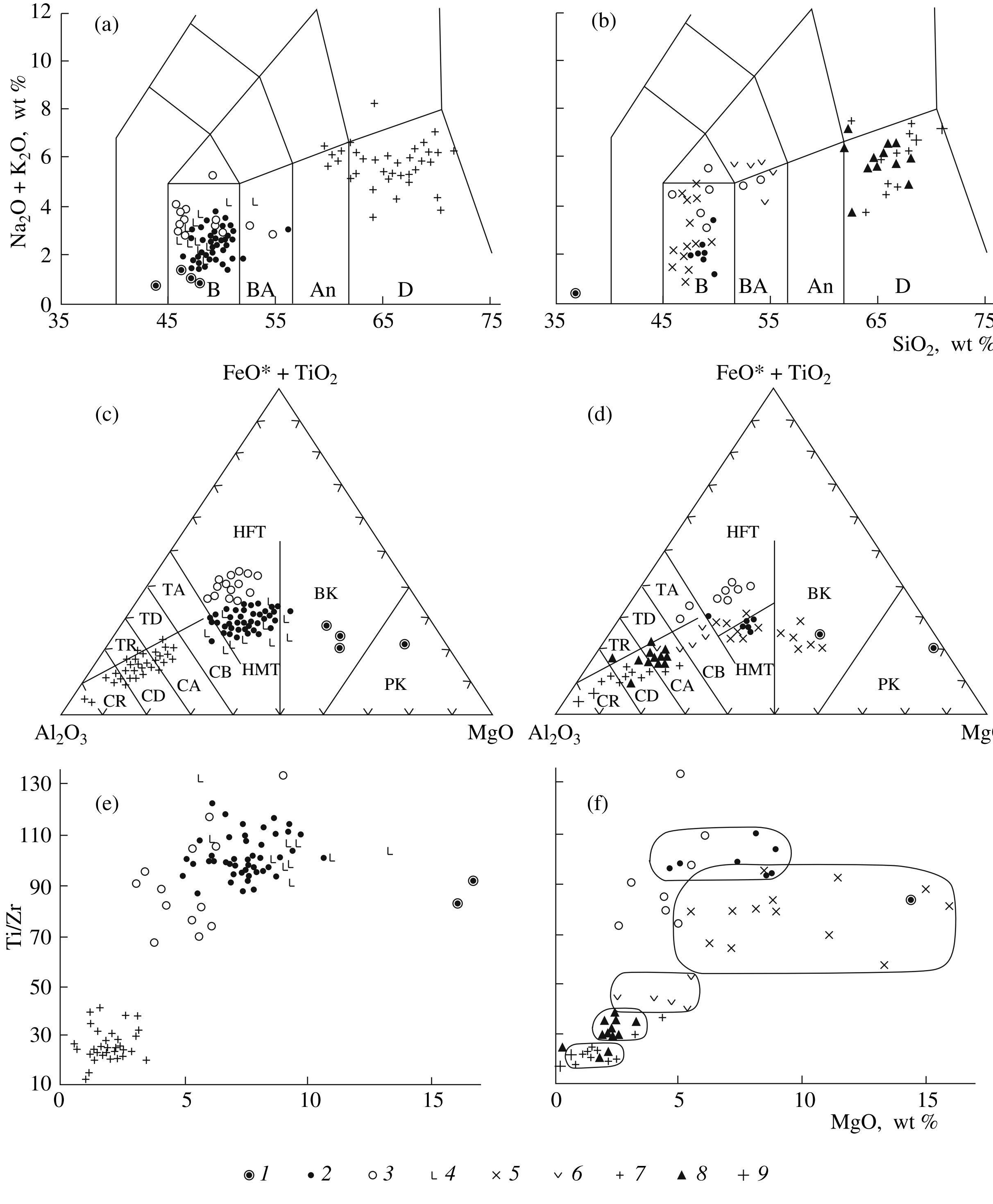

Fig. 3. Geochemical characteristics of metavolcanics from the (a, c, e) lower and (b, d, f) upper sequences of the Kalikorva structure in the $(Na_2O + K_2O)$–SiO_2 [14], Al_2O_3–$(FeO^*+ TiO_2)$–MgO [15], and Ti/Zr–MgO diagrams. (*1*) Metaperidotite, metapyroxenite, and komatiitic metabasalt; (*2*) tholeiitic metabasalt; (*3*) metagabbroid; (*4*) subalkaline metabasalt and metapicritic basalt; (*5*) subalkaline metabasaltic andesite; (*6*) metadacite (adakite); (*7*) HREE-enriched metadacite; and (*8*) trondhjemite. Fields: (a, b) B, basalts; BA, basaltic andesites; An, andesites; and D, dacites. (c, d) BK, basaltic komatiites; PK, peridotitic komatiites; HMT, highly magnesian tholeiites; TA, tholeiitic andesites; TD, tholeiitic dacites; TR, tholeiitic rhyolites; CB, calc-alkaline basalts; CA, calc-alkaline andesites; CD, calc-alkaline dacites; and CR, calc-alkaline rhyolites. Fields of rock types are outlined in Fig. 3f.

Table 1. Representative composition of major rock types from the lower sequences of the Kalikorva structure

Component	432/3	450/1a	450/6a	450/8	445/6	447/1	449/3	1127A	1679/1
	1	2	3	4	5	6	7	8	9
SiO_2	47.61	46.57	48.08	48.77	48.77	47.50	48.20	50.91	48.27
TiO_2	0.46	0.53	1.04	1.11	1.08	0.92	0.96	0.88	1.19
Al_2O_3	10.02	9.34	12.37	12.19	14.22	13.39	12.48	15.41	17.08
Fe_2O_3	12.95	13.49	14.42	15.00	15.46	16.24	14.60	11.84	11.89
MnO	0.24	0.20	0.20	0.20	0.27	0.24	0.15	0.16	0.29
MgO	16.00	13.60	8.52	9.14	6.98	9.32	9.61	7.70	6.84
CaO	11.63	14.38	12.54	11.38	11.15	10.61	11.63	11.67	12.23
Na_2O	0.90	1.08	1.97	1.88	1.68	1.59	1.72	1.54	2.09
K_2O	0.17	0.39	0.25	0.15	0.32	0.13	0.20	0.12	0.29
P_2O_5	0.02	<0.05	0.08	0.08	0.07	0.06	0.07	<0.05	–
Mg#	71	67	54	55	47	53	57	56	53
Ba	<100	242	167	100	<100	<100	220	<100	179
Rb	7	13	<5	<5	14	<5	8	<3	4
Sr	61	92	126	68	92	52	75	135	353
Hf	–	<0.5	1.5	1.3	1.2	0.74	1.8	1.9	2.0
Zr	32	20	50	52	65	52	46	55	65
Y	14	9	21	23	24	21	16	18	26
Nb	<5	<5	<5	<5	<5	<5	<5	4	5
Ta	–	0.09	0.13	<0.05	0.062	<0.03	0.14	0.13	0.16
Cr	2576	711	264	278	305	349	330	360	271
Ni	572	183	105	106	106	170	105	115	94
Co	83	74	57	52	64	83	49	62	57
Ti	2724	2917	5623	6036	6418	5468	5123	4899	5999
V	164	251	315	332	309	296	283	295	250
Sc	–	47.96	36.9	41.63	36.9	31.9	40.47	39.4	34.8
La	–	7.1	4.3	3.6	2.23	2.03	3.0	3.56	3.13
Ce	–	16.5	12	9.3	7.2	6.1	8.5	8.92	9.2
Nd	–	6.4	8.7	6.5	5.8	4.9	5.8	6.23	5.97
Sm	–	1.03	2.38	2.02	1.98	1.67	1.93	1.89	2.45
Eu	–	0.47	0.78	0.85	0.66	0.63	0.75	0.71	0.92
Tb	–	0.27	0.60	0.48	0.52	0.50	0.52	0.43	0.62
Yb	–	1.09	2.31	2.13	2.34	2.54	2.41	1.79	2.32
Lu	–	0.17	0.35	0.33	0.36	0.46	0.39	0.27	0.37
Th	–	<0.5	<0.5	<0.5	<0.5	<0.5	<0.5	<0.5	<0.5
REE	–	33.03	31.42	26.95	21.09	18.83	23.30	23.80	24.98
$(La/Yb)_n$	–	4.68	1.33	1.21	0.7	0.57	0.89	1.43	0.97
Zr/Y	2.28	2.22	2.4	2.26	2.70	2.48	2.80	3.05	2.5
Ti/Zr	85.12	145	118	112	99	105	111	89	92

Table 1. (Contd.)

Component	445/2	449/2	1679/3	1209·	445/5	450/7*	1602/2	122/2	171/1*
	10	11	12	13	14	15	16	17	18
SiO_2	49.18	46.86	54.80	46.63	64.12	64.28	66.05	68.37	72.08
TiO_2	2.01	2.00	2.47	0.58	0.67	0.43	0.44	0.69	0.58
Al_2O_3	13.09	11.46	13.51	16.67	16.72	17.10	17.74	13.52	12.92
Fe_2O_3	17.90	19.34	13.62	11.23	6.03	4.57	4.06	6.89	5.13
MnO	0.35	0.25	0.25	0.15	0.09	0.09	0.04	0.09	0.07
MgO	4.11	6.23	4.06	10.83	3.10	2.00	1.50	3.02	1.90
CaO	9.77	10.20	8.71	11.58	5.59	5.29	3.94	2.44	2.13
Na_2O	2.61	2.35	2.58	2.02	2.82	3.63	4.25	2.58	3.34
K_2O	0.75	0.44	0.24	0.52	0.65	2.44	1.79	2.31	1.78
P_2O_5	0.22	0.17	–	–	0.21	0.16	–	0.10	0.08
Mg#	31	39	40	66	51	47	43	–	–
Ba	<100	307	191	–	222	934	664	361	450
Rb	9	5	<3	30	23	52	43	82	36
Sr	145	202	160	190	574	424	451	192	311
Hf	–	2.4	3.2	–	3.0	–	2.9	–	2.8
Zr	175	81	149	36	124	110	106	98	79
Y	51	24	48	12	11	11	9	13	10
Nb	11	6	11	4	5	<5	6	6	<5
Ta	–	0.30	0.49	–	0.19	–	0.17	–	0.21
Cr	163	95	79	660	195	128	29	349	276
Ni	60	56	26	207	76	39	22	112	58
Co	60	63	48	70	28	<10	12	40	12
Ti	12049	11918	11948	3652	3931	2543	3327	4079	3437
V	394	560	453	203	99	78	96	136	91
Sc	–	39.44	37.0	–	7.87	7.74	7.23	–	11.0
La	–	9.4	9.03	–	20.4	21.20	18.3	–	11.5
Ce	–	20.1	26.0	–	44.6	43.62	34.7	–	23.8
Nd	–	10.8	18.6	–	23.9	22.54	23.1	–	12.3
Sm	–	3.29	5.61	–	3.71	3.38	3.12	–	1.96
Eu	–	1.17	1.70	–	0.93	1.18	0.97	–	0.74
Tb	–	0.58	1.1	–	0.29	0.34	0.25	–	0.24
Yb	–	2.38	3.93	–	0.57	0.76	0.70	–	0.93
Lu	–	0.33	0.58	–	<0.05	0.09	0.10	–	0.083
Th	–	1.3	<0.5	–	3.6	3.95	<0.5	–	2.4
REE	–	48.05	66.55	–	94.40	93.11	81.24	–	51.55
$(La/Yb)_n$	–	2.83	1.65	–	28.66	20.01	18.74	–	8.7
Zr/Y	3.43	3.4	3.1	3.0	11.27	10	11.8	7.54	7.9
Ti/Zr	68.8	147	97	101	31.7	23.11	25	41.6	43.5

Notes: Rocks: (1) metapyroxenite, (2) komatiitic metabasalt, (3–9) Mg tholeiitic metabasalts, (10–12) Fe tholeiitic metabasalts, (13) metagabbro, (14–16) metadacites (adakites), and (17–18) metagraywackes. Major elements were determined by X-ray spectral analysis at the Karpinskii All-Russia Research Institute of Geology. Trace elements were determined by XRF on a VRA-2 analyzer at the Institute of Precambrian Geology and Geochronology, Russian Academy of Sciences (St. Petersburg). REE were analyzed by INAA at the Institute of Precambrian Geology and Geochronology, Russian Academy of Sciences, on a TNAA instrument. Oxides are given in wt %, and trace elements are in ppm. Dashes denote not determined. All analyses were recalculated on a dry basis. All iron is calculated as Fe_2O_3.

* Analyses of dated samples.

Table 2. Representative compositions of major rock types from the upper sequence of the Kalikorva structure

Component	59/6	35/8	43/8	58/4b	35/9	43/2	58/4a	74/2	43/3	43/4	35/12b	35/12a
	1	2	3	4	5	6	7	8	9	10	11	12
SiO_2	43.87	47.32	46.86	47.54	49.07	48.50	48.02	48.94	48.32	54.65	46.21	45.90
TiO_2	0.24	0.58	0.38	0.51	0.99	0.99	0.94	0.93	1.88	1.88	0.75	0.74
Al_2O_3	1.38	11.40	8.11	11.45	14.02	15.86	14.31	15.11	14.40	16.16	11.70	12.20
Fe_2O_3	15.71	13.99	13.62	13.55	14.79	13.31	14.40	13.86	17.36	11.04	12.63	12.34
MnO	0.32	0.27	0.23	0.23	0.23	0.19	0.22	0.17	0.19	0.15	0.22	0.22
MgO	32.52	14.48	17.46	15.10	7.52	8.25	8.72	8.97	6.44	3.88	15.97	11.63
CaO	11.23	10.59	11.42	10.30	11.23	10.43	11.32	9.27	8.94	8.27	10.60	14.62
Na_2O	0.17	1.23	1.02	1.10	1.94	2.20	1.74	2.51	3.11	5.26	1.09	1.25
K_2O	0.02	0.12	0.04	0.21	0.16	0.23	0.24	0.18	0.61	0.25	0.62	0.89
P_2O_5	0.03	0.02	<0.05	<0.05	0.07	0.06	0.07	0.07	0.15	0.19	0.20	0.20
Mg#	77	68	72	70	53	55	54	56	38	36	72	65
Ba	0	49	<100	0	15	<100	0	0	<100	284	153	149
Rb	1	6	<5	8	3	8	7	7	23	<5	21	34
Sr	147	93	76	92	114	117	109	107	300	272	286	550
Hf	–	1.2	–	–	2.1	0.91	–	–	2.8	4.0	–	1.6
Zr	16	42	27	35	60	54	60	54	120	153	56	48
Y	3	14	10	13	26	21	23	21	26	31	16	19
Nb	2	1.6	<5	1.6	3.2	<5	3	3	12	16	3	4
Ta	–	0.086	–	–	0.15	0.087	–	–	0.62	0.77	–	0.12
Cr	2796	1718	1862	1428	291	410	279	398	92	60	1256	1163
Ni	1932	463	405	388	148	164	149	142	59	55	385	375
Co	119	59	59	82	51	52	39	43	64	73	54	50
Ti	1266	3442	2555	3008	5804	5916	5596	5520	11297	11312	4443	4389
V	50	172	179	158	304	253	262	272	334	396	223	188
Sc	–	34.1	–	–	46.6	24.7	–	–	20.7	25.3	–	31.2
La	–	2.81	–	–	3.40	2.27	–	–	12.6	16.9	–	11.3
Ce	–	6.2	–	–	8.9	6.4	–	–	32	42.7	–	27.8
Nd	–	4.6	–	–	6.7	5.7	–	–	23.2	31.7	–	17.5
Sm	–	1.53	–	–	2.71	2.03	–	–	5.46	6.89	–	3.99
Eu	–	0.49	–	–	0.98	0.69	–	–	1.68	1.99	–	1.20
Tb	–	0.38	–	–	0.56	0.50	–	–	0.89	1.10	–	0.53
Yb	–	1.49	–	–	2.68	2.00	–	–	2.23	3.95	–	1.39
Lu	–	0.22	–	–	0.42	0.30	–	–	0.30	0.40	–	0.20
Th	–	<0.5	–	–	<0.5	<0.5	–	–	<0.5	0.84	–	0.75
REE	–	18.0	–	–	26.35	19.90	–	–	78.36	104.63	–	64.66
$(La/Yb)_n$	–	1.36	–	–	0.87	0.81	–	–	4.07	4.17	–	5.85
Zr/Y	5.3	3.0	2.7	2.69	2.31	2.57	2.61	2.53	4.6	4.93	3.5	2.52
Ti/Zr	79.1	82	94.6	85.9	96.7	109	93.3	102.2	94	73.9	79.3	91.4

Table 2. (Contd.)

Component	60/1	35/10·	58/12	59/1	35/10	35/11	35/10a	43	58/1	59/2*	60/6	58/3
	13	14	15	16	17	18	19	20	21	22	23	24
SiO_2	48.33	47.05	47.70	48.31	55.67	53.76	68.10	65.17	63.94	68.16	66.13	64.44
TiO_2	0.75	1.04	1.12	1.13	0.79	0.86	0.39	0.43	0.62	0.41	0.48	0.72
Al_2O_3	13.09	14.45	16.12	15.93	18.09	19.59	16.49	16.48	16.40	16.37	15.83	16.92
Fe_2O_3	12.51	14.32	13.74	13.08	8.80	8.44	3.26	4.65	5.81	3.19	4.68	5.83
MnO	0.24	0.28	0.32	0.24	0.18	0.13	0.06	0.07	0.10	0.04	0.09	0.08
MgO	11.19	8.17	6.27	5.62	4.11	2.59	1.41	1.52	4.20	1.50	2.51	2.25
CaO	11.26	10.87	10.19	9.94	6.79	8.36	4.01	5.88	5.13	3.37	5.24	3.95
Na_2O	1.30	2.71	2.53	3.89	2.89	3.35	4.26	3.53	1.22	5.02	3.08	3.95
K_2O	1.08	0.81	1.67	1.53	2.46	2.56	1.80	2.13	2.43	1.77	1.68	1.67
P_2O_5	0.24	0.29	0.34	0.34	0.21	0.36	0.22	0.14	0.16	0.17	0.29	0.19
Mg#	65	53	48	46	48	43	46	40	59	58	60	54
Ba	567	288	480	532	1018	545	822	778	705	781	894	454
Rb	29	8	34	54	60	85	57	78	85	43	68	59
Sr	381	675	523	711	693	1064	912	561	390	557	851	483
Hf	–	1.8	2.5	2.7	3.1	–	3.4	–	2.2	2.5	–	3.8
Zr	65	77	102	84	107	115	110	101	101	103	141	141
Y	19	29	29	26	17	31	8	11	11	9	20	17
Nb	4	5	6	4.3	3.5	6	2.5	3	4	3	5	7
Ta	–	0.16	0.18	0.23	0.14	–	0.23	–	0.15	0.14	–	0.29
Cr	710	295	119	89	88	129	53	50	125	60	106	164
Ni	99	116	35	31	25	34	23	23	52	29	36	61
Co	46	32	25	37.5	19	27	<10	21	20	0	11	23
Ti	4432	6101	6614	6565	4609	5113	2302	2475	3607	2388	2769	4226
V	241	279	295	295	142	216	50	61	119	41	91	114
Sc	–	38	27.3	26.3	5.67	–	5.9	–	12.4	5.0	–	14.2
La	–	14	18.3	15.1	40.6	–	43	–	18.2	31.0	–	29.6
Ce	–	36	39.9	33.8	83.6	–	97	–	35.0	62.6	–	62.8
Nd	–	25	27.0	20.2	39.4	–	37	–	19.0	28.8	–	28.9
Sm	–	5.43	5.89	4.88	5.21	–	5.45	–	2.96	3.79	–	5.29
Eu	–	1.55	1.82	1.40	1.21	–	1.15	–	0.94	0.93	–	1.27
Tb	–	0.80	0.92	0.77	0.42	–	0.47	–	0.29	0.28	–	0.62
Yb	–	2.4	2.66	2.56	0.73	–	0.71	–	0.76	0.49	–	1.47
Lu	–	0.32	0.34	0.36	0.088	–	0.10	–	<0.05	<0.05	–	0.11
Th	–	<1.0	2.0	<0.5	7.0	–	6.4	–	2.5	4.5	–	6.1
REE	–	85/50	96.83	79.08	171.26	–	184.88	–	77.09	127.89	–	130.06
$(La/Yb)_n$	–	4.2	4.93	4.26	39.76	–	44.28	–	19.25	44.8	–	–
Zr/Y	3.42	2.66	3.52	3.23	6.29	3.71	13.75	9.18	9.2	11.2	7.05	8.29
Ti/Zr	91.43	79.2	64.8	78.15	43.07	44.46	20.92	24.50	35.7	23.18	19.64	30

Table 2. (Contd.)

Compo-nent	58/7	77/1	77/8a	78/6	58/2	60/4	76/2	40/1	149/1	321/1	1241
	25	26	27	28	29	30	31	32	33	34	35
SiO_2	68.27	62.47	65.86	66.40	63.45	69.57	64.40	71.54	70.86	71.57	70.20
TiO_2	0.47	0.72	0.80	0.64	0.81	0.62	0.79	0.33	0.42	0.24	0.28
Al_2O_3	15.76	16.99	16.09	17.13	16.77	13.92	15.99	16.19	15.25	15.32	15.90
Fe_2O_3	4.88	6.46	5.19	2.90	7.79	5.65	6.95	2.00	3.16	2.35	2.37
MnO	0.04	0.10	0.08	0.04	0.10	0.07	0.10	0.03	0.04	0.03	0.02
MgO	1.86	3.37	2.12	1.98	3.58	2.24	3.12	0.10	1.21	0.81	0.67
CaO	2.81	6.09	3.04	4.31	2.81	2.52	3.36	2.73	2.86	2.40	2.55
Na_2O	4.81	1.29	4.65	4.72	2.60	3.16	3.20	5.68	4.36	5.01	4.84
K_2O	0.98	2.31	2.02	1.73	1.98	2.15	1.97	1.34	1.70	2.24	2.85
P_2O_5	0.11	0.20	0.17	0.20	0.10	0.10	0.11	0.06	0.14	0.10	0.11
Mg#	43	51	45	58	–	–	–	39	43	40	36
Ba	233	692	378	415	444	252	459	450	513	450	1005
Rb	42	77	62	67	68	139	90	49	83	65	71
Sr	456	455	443	399	192	200	262	583	443	381	481
Hf	3.4	3.9	3.7	3.5	–	–	2.5	3.3	3.9	3.4	3.6
Zr	138	120	137	134	119	103	120	116	147	84	126
Y	14.5	14	14	16	16	11	15	7	9	9	6
Nb	7	4	6	7	5	5	6	3.4	6	<5	6
Ta	0.35	0.17	0.36	0.37	–	–	0.22	0.18	0.27	0.15	0.17
Cr	80	138	182	214	361	310	297	86	115	37	52
Ni	50	40	55	19	50	100	114	18	34	28	18
Co	24	26	25	16	21	23	28	<10	<10	<10	<10
Ti	2697	4131	4670	3759	4714	3626	4599	1995	2490	1477	1685
V	58	130	125	114	166	131	153	48	42	<30	<30
Sc	10.8	15	14.8	15	–	–	20	2.1	4.2	3.52	2.74
La	30.5	25	25.0	8.3	–	–	21	16.0	20.4	13.4	28.6
Ce	67.3	53	62.2	20.0	–	–	52	27.3	40.7	28.0	53.4
Nd	33.3	30	34.1	9.0	–	–	25	12.8	19.9	10.9	22.0
Sm	4.89	5.37	4.68	2.06	–	–	4.19	1.51	2.72	2.15	2.59
Eu	1.03	1.26	1.54	0.55	–	–	0.98	0.52	0.70	0.55	0.83
Tb	0.54	0.63	0.43	0.44	–	–	0.71	0.14	0.24	0.27	0.20
Yb	1.41	1.30	1.36	1.4	–	–	1.7	0.24	0.47	0.35	0.29
Lu	0.10	0.18	0.17	0.21	–	–	0.23	<0.05	<0.05	<0.1	<0.1
Th	10.4	4.0	6.0	6.2	–	–	4.0	3.9	4.6	2.2	4.4
REE	139.07	116.74	135.48	48.6	–	–	106.2	58.51	85.66	55.62	107.91
$(La/Yb)_n$	16.0	13.81	13.2	4.37	–	–	9.9	47.85	28.66	27.14	71.84
Zr/Y	9.52	8.57	9.8	8.37	7.4	9.4	8.0	16.57	16.33	9.3	21.0
Ti/Zr	19.54	34.42	34.0	28.0	39.61	35.20	38.32	17.19	16.94	17.58	13.4

Note: Rocks: (1) metaperidotite, (2–4) komatiite metabasalts, (5–8) Mg-tholeiite metabasalts, (9–10) Fe metabasalts, (11–16) subalkaline metabasalts and picritic basalts, (17–18) subalkaline metabasaltic andesite, (19–23) metadacites (adakites), (24–28) HREE enriched metadacites, (29–31) metagraywackes, and (32–35) trondhjemites. Other notes are the same as in Table 1.

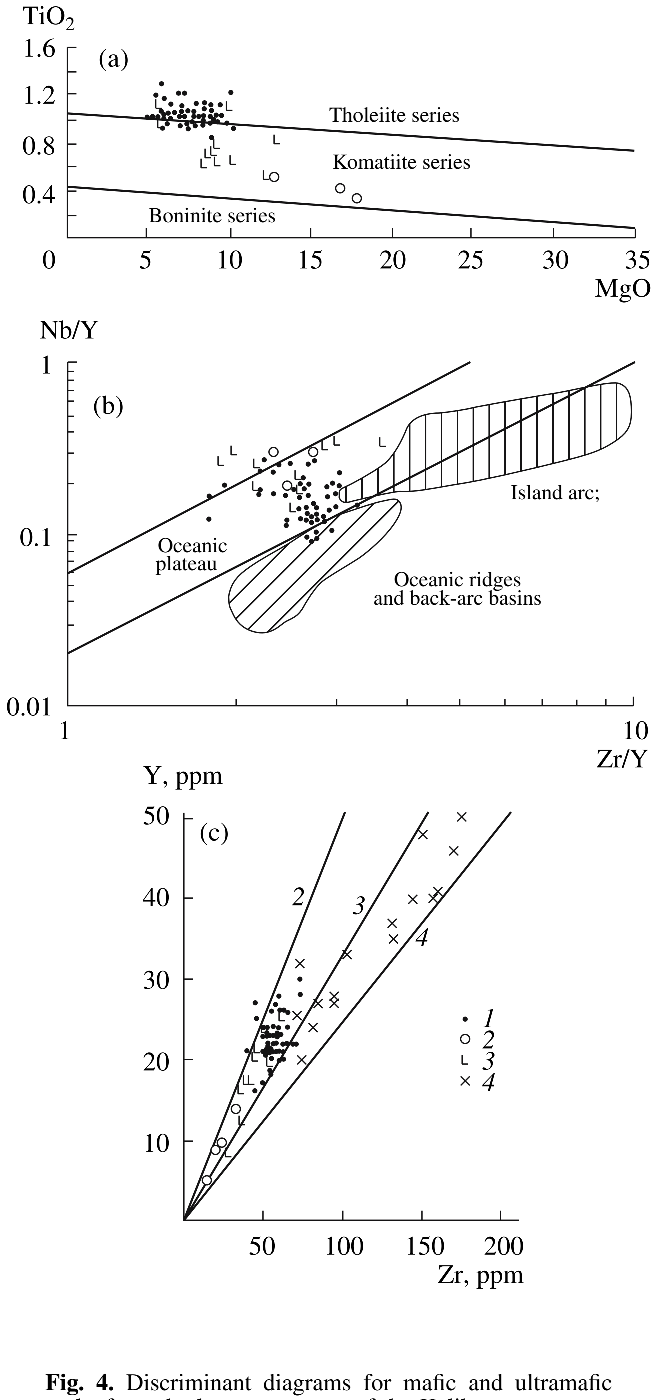

Fig. 4. Discriminant diagrams for mafic and ultramafic rocks from the lower sequence of the Kalikorva structure. (a) MgO–TiO_2 [17]. (b) Zr/Y–Nb/Y [18]. (c) Zr–Y. (*1*) Mg tholeiitic metabasalt, (*2*) komatiitic metabasalt and metapyroxenite, (*3*) Fe tholeiitic metabasalt, and (*4*) metagabbro.

Ta and Nb anomalies; and small Ti, Zr, and Hf anomalies.

Metagraywackes compose a significant portion of the supracrustal sequences among felsic and intermediate rocks, especially in the upper sequences, and were described in detail by Myskova et al. [13]. They were classified as immature rocks with model sources containing up to 50% mafic volcanics. Compared with the felsic and intermediate volcanics, they show considerable variations in SiO_2, Al_2O_3, and TiO_2 contents, high MgO and low CaO contents (i.e., elevated Mg/Ca ratios), lower Sr, and, primarily, high contents of Cr (up to 400 ppm) and other transition elements. In this paper, the compositions of metagraywacke are presented to characterize the entire rock association and compare them with the intermediate volcanics (Tables 1, 2; Fig. 7). The metagraywackes are similar to the volcanic rocks in REE distribution patterns (sample 171) but are less enriched in LREE (Fig. 6).

Upper sequence. Tholeiitic metabasalts occur as thin layers (m = 1, 2, 6, and 9 m) in thin alternation units or among metagraywackes. They contain from 7.52 to 8.97 wt % MgO, from 291 to 410 ppm Cr, from 148 to 164 ppm Ni, and from 50 to 60 ppm Zr. These rocks have *Mg#* values ranging from 53 to 58 and nearly chondritic ratios (average of 7 analyses) of Ti/Zr = 98, Zr/Y = 2.68, Al_2O_3/TiO_2 = 15.47, Ti/Y = 262.3, and Zr/Sm = 22–26.

Komatiitic metabasalts occur as rare thin (tens of centimeters) interlayers among metabasalts and contain from 14.48 to 17.41 wt % MgO, from 1428 to 1862 ppm Cr, from 388 to 463 ppm Ni, and from 27 to 42 ppm Zr. They show *Mg#* = 68–72 and MORB-like ratios of Ti/Zr = 82–102, Zr/Y = 2.61–3.0, Al_2O_3/TiO_2 = 16–21, Ti/Y = 231–255, and Zr/Sm = 22–27 and are probably comagmatic with the tholeiites.

Rare intrusive bodies (*m* = 1–2 m) of metaperidotites with high contents of MgO (32–52 wt %), Cr, Ni, and Co but low Al_2O_3 (1.32 wt %) are probably cumulate rocks (Table 2, sample 59/6).

The Fe–Ti tholeiites associate with tholeiitic and komatiitic basalts, basaltic andesites, and dacites. They have low MgO from 3.51 to 6.44 wt %, from 27 to 92 ppm Cr, from 50 to 68 ppm Ni, elevated contents of Fe_2O_3*tot* (from 10.54 to 17.93 wt %), from 334 to 408 ppm V, and high Nb contents from 11 to 16 ppm, which are significantly higher than in their analogues from the lower sequences. Their average Ti/Zr ratio of 95 is close to the chondritic value. The Ti/Y (from 364 to 565, averaging 431) and Zr/Y (from 3.9 to 5.2, averaging 4.6) ratios are significantly higher than the chondritic values. The enrichment of melanocratic rocks in MgO and Fe_2O_3*tot* and leucocratic rocks in SiO_2, Al_2O_3, and K_2O presumably results from fractional crystallization. The compositions of these rocks are similar to those of the Late Archean Fe tholeiites of the Hisovaara structure [9].

The subalkaline basalts and picritic basalts form interlayers, 1–20 cm thick, occasionally up to 1.0–1.5 m in thin alternations with dacites, tholeiite and komatiitic basalts. This is probably a differentiated dike complex with MgO varying from 15.97 to 6.27 wt %, from 119 to 1256 ppm Cr, and *Mg#* from 72 to 46. They are char-

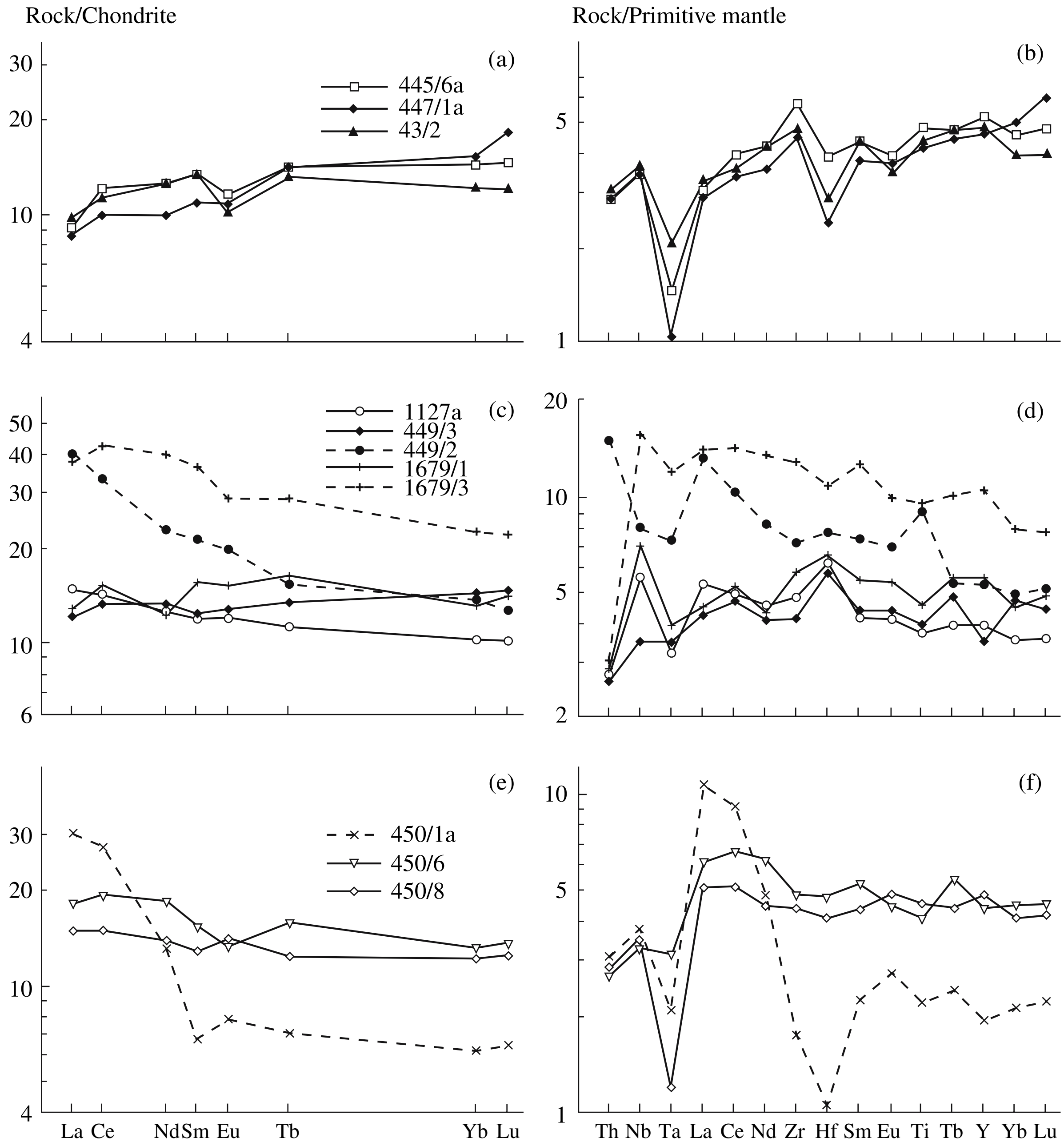

Fig. 5. Chondrite- and mantle-normalized [21] REE and trace element distribution patterns for metabasalts from the lower sequence of the Kalikorva structure. (a, b) Magnesian basalts with Eu anomalies. (c, d) Magnesian basalts compared with Fe basalts. (e, f) Compositional variations of rocks from a single outcrop. Sample numbers correspond to the numbers of chemical analyses in Tables 1 and 2.

acterized by elevated contents of K_2O, P_2O_5, Sr, Ba, and REE at high and weakly variable TiO_2 (from 0.75 to 1.13 wt %) and Fe_2O_3*tot* (from 12.34 to 14.32 wt %).

Subalkaline basaltic andesites are the least abundant rocks, which also occur in thinly alternating units. They are distinguished by high contents of Al_2O_3 (18.09–19.59 wt %), K_2O (2.41–2.56 wt %), P_2O_5 (0.21–0.31 wt %), Ba, Sr, and REE and low contents of MgO (2.59–4.11 wt %), Cr (88–129 ppm), and Ni (19–27 ppm).

Metadacites are the most widespread rocks in the upper sequence. They occur both in the units of thin alternation and as individual interlayers among the graywackes. The dacites are subdivided into two groups, which are similar in major element composi-

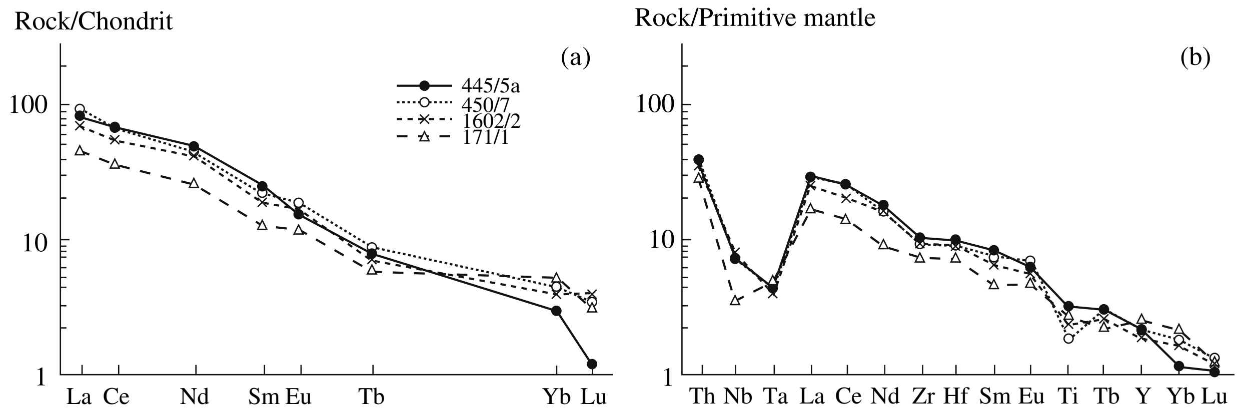

Fig. 6. Chondrite- and primitive mantle-normalized [21] REE and trace-element distribution patterns for metadacites from the lower sequence of the Kalikorva structure compared with metagraywackes (sample 171/1). Sample numbers correspond to those of chemical analyses in Table 1.

tion but differ in trace-element characteristics. The first group includes aluminous dacites with high contents of Ba, Rb, and Sr, low contents of Y and Yb, and superchondritic Sr/Y and Zr/Sm ratios. They can be ascribed to adakites and are similar to the rocks of the lower sequence. In the Sr/Y–Y diagram (Fig. 8), they plot in the field of high-Al TTD, which are formed by partial melting of Archean mafic sources corresponding to garnet amphibolite. The second group is characterized by lower Sr (but higher than 400 ppm) and elevated contents of Zr (from 120 to 141 ppm), Y (from 14 to 17 ppm), Nb (from 4 to 7 ppm), Cr (from 80 to 214 ppm), and Yb (from 1.30 to 1.47 ppm). Owing to the elevated contents of Cr and HREE [10, 13], some of these rocks were ascribed to metagraywackes. In the variation diagrams (Fig. 7b), they are intermediate between dacites (adakites) and metagraywackes, showing the signatures of both rock types. These rocks typically occur in thinly alternating units, which show a wider diversity of magmatic rocks, and are higher in CaO and Sr than the graywackes. Like the adakites, they show CaO > MgO. All these observations suggest their dacitic affinity. In the Sr/Y–Y diagram (Fig. 8), the points of these rocks mainly fall within the field of low-Al island-arc andesite–dacite–rhyolite (ADR) assemblage, which is formed by fractionation. The model source of these rocks is different from that of adakites and corresponds to a garnet-free amphibolite (Fig. 9).

Thus, the upper sequence displays a wide diversity in magmatic rock types. This can be seen in the Ti/Zr–MgO diagram (Fig. 3f), in which each type shows its own Ti/Zr ratio and, hence, has a specific source. This is also demonstrated by their REE distribution patterns (Fig. 10).

Figures 10a and 10b show REE distribution patterns for tholeiitic basalts, komatiitic basalts, subalkaline picritic basalts, and subalkaline basaltic andesites from a single exposure.

The tholeiitic and komatiitic basalts display unfractionated parallel REE patterns with REE contents 10 and 15 times chondrite, respectively. The picritic basalts are more enriched in REE (REE total from 64–66 to 85.5 ppm) and show $(La/Yb)_N$ = 4.20–5.85. The basaltic andesites have the steepest patterns with strong LREE enrichment (LREE total of 171.26 ppm) and HREE depletion, $La/Yb)_N$ = 39.76.

In the primitive mantle-normalized spidergram (Fig. 10b), the tholeiitic and komatiitic basalts have flat REE patterns and very slight negative Ta–Nb and Ti anomalies. The other rocks have three distinct negative anomalies (Ta–Nb, Zr–Hf, and Ti), which are indicative of the island-arc affinity.

Figures 10c and 10d show two groups of dacites. It can be seen that the second group is relatively enriched in HREE. The spidergram displays distinct negative Nb–Ta and Ti anomalies and a weaker Zr–Hf anomaly. The REE distribution patterns of trondhjemites are shown for comparison (Figs. 10e, 10f). Sample 40/1 was taken from the sequences, and others were sampled from a tonalite field east of the structure considered [11]. These rocks are chemically classified as adakites (Table 2). The REE distribution patterns of tonalites are similar to those of dacites, whereas the trondhjemites are more HREE depleted and contain from 0.24 to 0.47 ppm Yb.

The Fe–Ti basalts have moderately fractionated REE patterns (Figs. 10g, 10h) with $(La/Sm)_N$ = 1.47–1.58, $(La/Yb)_N$ = 4.07–4.17, and La/Nb = 1. In terms of these characteristics, they are similar to the Fe–Ti basalts of Hisovaara [9], which have $(La/Sm)_N$ = 1.4, $(La/Yb)_N$ = 3.05, and La/Nb = 1.3, and different from Proterozoic Fe drusites, which are depleted in Nb, enriched in REE, and have steeper distribution patterns [25].

Thus, the upper sequence consists of tholeiite series rocks intercalated with calc-alkaline and subalkaline rocks of island-arc affinity. Such a diversity of igneous rock types is characteristic of back-arc basins. The Nb-enriched Fe–Ti basalts form a separate group. Similar rocks occur in modern island arc systems together with adakites and Mg andesites. This rock association is an indicator of subduction settings. Such Fe–Ti basalts are generated by melting of a Nb-rich phase, such as amphibole or ilmenite, owing to the adakite metasomatism of a mantle wedge [26, 27]. The presence of subalkaline picritic basalts and basaltic andesites in addition to HREE enriched dacites, whose magmas are formed via crystallization differentiation, provides evidence for a more mature island arc stage.

U–PB ZIRCON DATING

U–Pb zircon ages were estimated for two metadacite samples from the lower and upper sequences and one metagraywacke sample from the Kalikorva structure. We also determined the zircon age of metatuff from the adjacent Kichany structure of the Tikshozero greenstone belts. Sampling sites are shown in Fig. 1.

The U–Pb isotopic analysis of zircon was carried out on a SHRIMP-II ion microprobe at the Center of Isotopic Research, Karpinskii All-Russia Research Institute (St. Petersburg). The data were processed following the procedure described in [28] using the SQUID [29] and Isoplot/Ex [30] programs. The Pb/U ratios were normalized to a $^{206}Pb/^{238}U$ of 0.0665 in the TEMORA standard zircon corresponding to an age of 416.7 ± 1.30 Ma (2σ) [31]. The measurement results are shown in Fig. 11 and Table 3.

Metadacite from the upper sequence (sample 59/2). A monomineralic zircon fraction consisted of prismatic and long-prismatic light pink subhedral crystals, partially dissolved and overgrown by thin shells. They have a fine zoned structure, high birefringence, and contain rounded, probably melt, inclusions. The crystal size is 40–130 μm, and the elongation ratio is 2.5–4.0. The cathodoluminescent images of zircons exhibit thinly zoned cores (Fig. 11a) and black or gray shells, probably of late magmatic origin. Many zircons contain altered domains both in cores and rims, which are distinguished by completely or partially obliterated zoning and brighter cathodoluminescence. The U content of the zoned crystals is 99–336 ppm and Th/U = 0.34–0.86. The altered zircons have U = 118–1550 ppm and Th/U = 0.12–0.32. Areas with magmatic zoning were selected for local U–Pb dating. The eight-point concordant age of zircon is 2785±13 13 Ma (Fig. 11a), which is interpreted as magmatic age.

Metadacite from the lower sequence (sample 450/7). Zircons are prismatic subhedral light pink crystals of uneven coloration. The grain size varies within 40–150 μm with the predominance of fine fractions smaller than 80 μm. The elongation ratio is 2.5–4.0. The grains typically contain zoned fragments, usually in the central parts, and unzoned rims. The cathodoluminescent images of zircons reveal areas with magmatic zoning in the core and homogenous rims with bright luminescence (Fig. 11b). The irregular and intricate boundaries between the zoned and homogenous areas indicate extensive recrystallization of magmatic zircon under high-temperature metamorphic conditions.

The areas with magmatic zoning and surrounding homogenous shells were dated separately. The Th/U ratios of measured zoned areas are 0.38–0.67, which corresponds to magmatic zircon. The U–Pb age of thinly zoned zircons obtained on the upper intercept of six-point discordia (Table 3) is 2770 ± 12 Ma (Fig. 11b) and can be considered as the age of magmatism. The Th/U ratios of the shells are 0.01–0.05, which is typical of metamorphic zircons. A five-point discordia yields a shell age of 1821 ± 39 Ma (Table 3, Fig. 11c).

Metagraywacke from the lower sequence (sample 171/1). A monomineral zircon fraction is represented by turbid and transparent subhedral thinly zoned crystals with acicular inclusions. The sample contains numerous fragments of prismatic crystals. The crystal size varies from 120 to 40 μm with an elongation ratio of 2–3. In addition, there are transparent colorless zircons without inclusions with a grain size of 30–70 μm and an elongation ratio of 1.4–2.0. Cathodoluminescent images show that the prismatic zircons have a thinly zoned structure with traces of recrystallization (Fig. 11d, I), and rounded grains bear relics of zoning (Fig. 11d, II). Both zircon types have similar U contents varying within 57–243 ppm and a Th/U ratio of 0.51–0.26, which indicates their primary magmatic rather than metamorphic origin.

The upper intercept age of discordia constructed for all zircon types is 2766 ± 21 Ma (Fig. 11d), which can be considered as the protolith age.

Metatuff from the volcanic sequence of the Tikshozero greenstone belt, Kichany area (sample 1253/2). A monomineralic zircon fraction is represented by transparent pale pink and semitransparent pinkish brown subhedral prismatic and rounded crystals and fragments. Many grains are rimmed by irregular thin turbid brown shells. The crystals are 40–150 μm in size and have an elongation ratio of 1.2–2.0. Cathodoluminescent images reveal predominant zoned (Fig. 11e) and partly recrystallized grains, occasionally with dark cores. Many grains are overgrown by black shells. The zoned zircons have U = 45–165 ppm and Th/U = 0.44–0.66, whereas the dark shells have U = 364–800 ppm

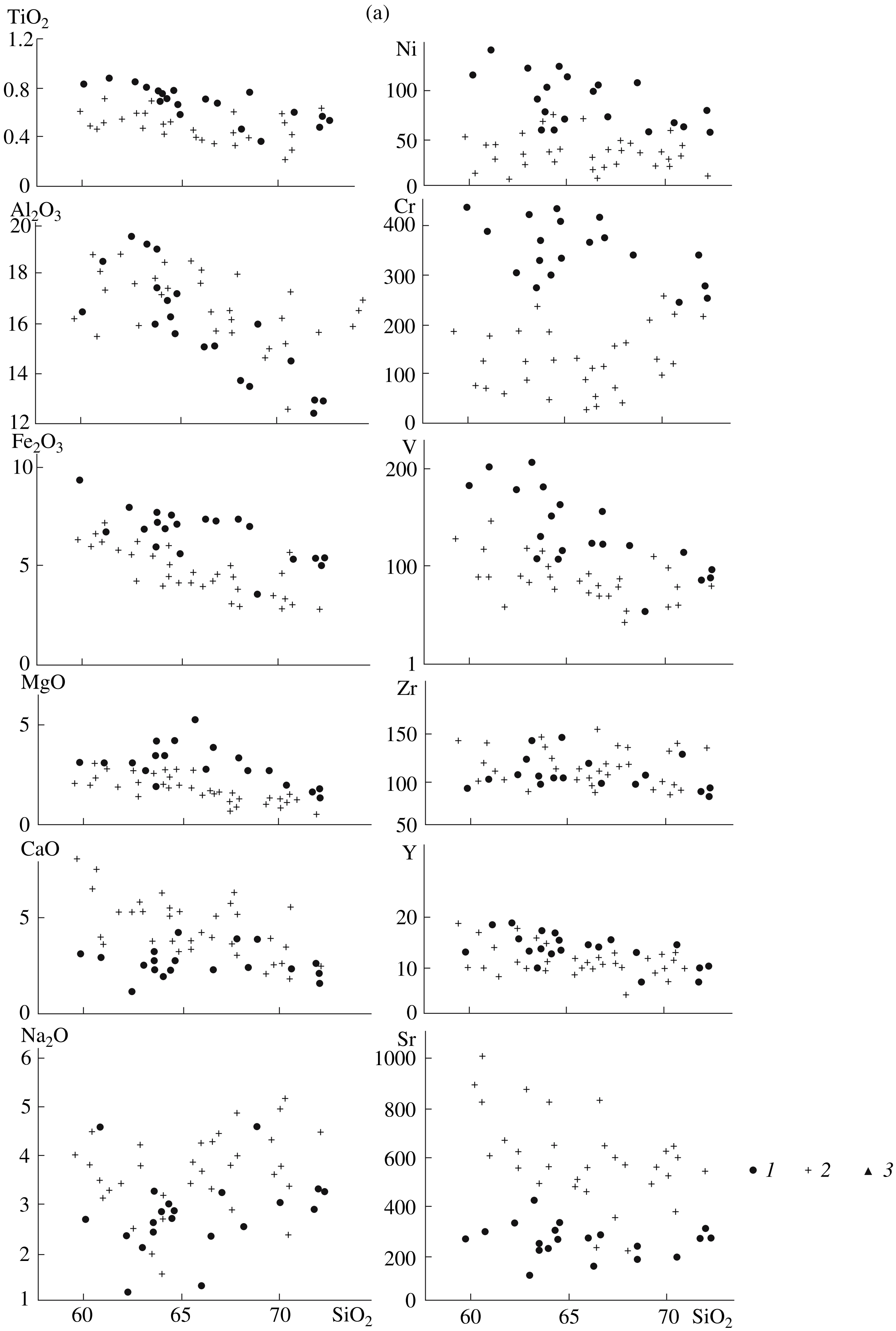

Fig. 7. Diagrams SiO_2–element for the rocks of the (a) lower and (b) upper sequences of the Kalikorva structure. (*1*) metadacite (adakite), (*2*) HREE-enriched metadacite, and (*3*) metagraywacke.

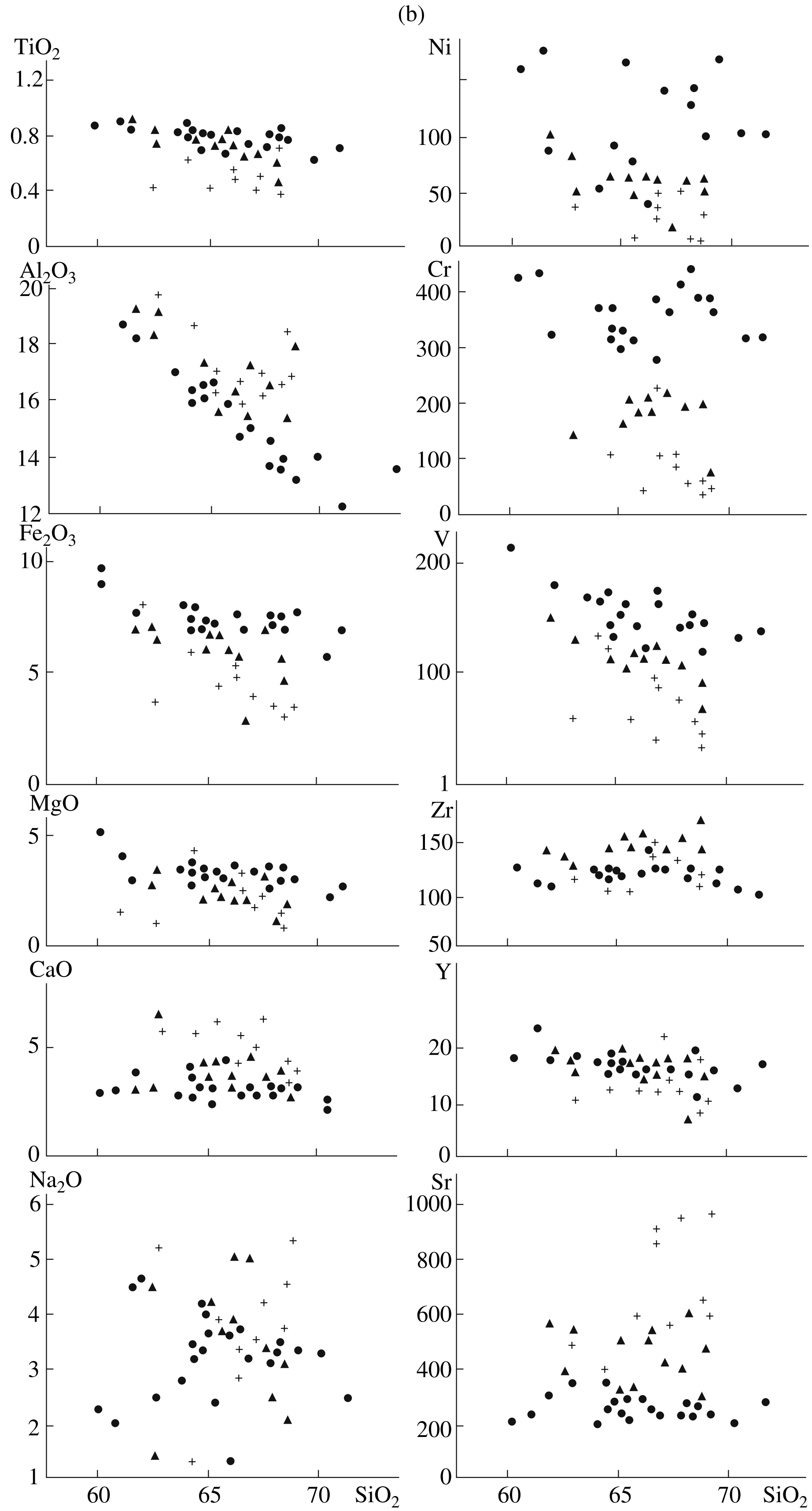
(b)
TiO2
1.2
0.8
0.4
0
Ni
100
50
0
Al2O3
20
18
16
14
12
Cr
400
300
200
100
0
Fe2O3
10
5
0
V
200
100
1
MgO
5
0
Zr
150
100
50
CaO
5
0
Y
20
10
0
Na2O
6
5
4
3
2
1
Sr
1000
800
600
400
200
0
60
65
70
SiO2
60
65
70
SiO2

Fig. 7. Contd.

Table 3. U–Pb isotope data for zircon from the gneisses of the Kalikorva structure

Point	% $^{206}Pb_c$	ppm U	ppm Th	$^{232}Th/^{238}U$	ppm $^{206}Pb^*$	$^{206}Pb/^{238}U$ age	$^{207}Pb/^{206}Pb$ age	$^{208}Pb/^{232}Th$ age
450/7, metadacite								
Core								
1.2	0.02	211	129	0.63	88.1	2552 ± 80	2765 ± 8	2498 ± 97
3.2	0.23	123	79	0.67	52.9	2607 ± 81	2790 ± 10	2497 ± 99
5.2	0.02	149	72	0.50	64.2	2616 ± 82	2767 ± 9	2559 ± 100
6.2	0.24	159	58	0.38	66.8	2558 ± 80	2757 ± 10	2451 ± 10
8.2	0.03	139	69	0.51	60.1	2626 ± 83	2760 ± 9	2656 ± 110
9.2	0.09	166	84	0.52	72.2	2642 ± 82	2781 ± 9	2645 ± 100
Shell								
2.1	0.34	63	0	0.00	19.7	1997 ± 70	1784 ± 37	
3.1	2.49	12	1	0.05	4.23	2098 ± 77	1796 ± 120	
4.1	1.93	94	2	0.02	29.3	1966 ± 65	1829 ± 42	
5.1	0.42	41	2	0.04	9.73	1566 ± 54	1836 ± 37	
7.1	1.38	89	1	0.01	30.4	2141 ± 70	1856 ± 46	
59/2, metadacite								
1.1	0.11	190	59	0.32	73.6	2395 ± 24	2607 ± 27	2525 ± 84
1.2	0.14	336	126	0.39	156	2789 ± 18	2816 ± 11	2661 ± 59
2.1	0.36	99	40	0.41	45.5	2766 ± 60	2773 ± 22	2755 ± 30
3.1	–	167	75	0.47	78.2	2812 ± 39	2823 ± 15	2855 ± 72
4.1	0.44	119	37	0.32	55.4	2773 ± 29	2720 ± 21	2858 ± 130
5.1	0.20	212	84	0.41	98.7	2785 ± 23	2805 ± 14	2770 ± 73
5.2	0.08	1550	297	0.20	513	2098 ± 8	2651 ± 7	2010 ± 28
6.1	0.31	102	41	0.42	51.9	2982 ± 38	2754 ± 23	2962 ± 110
6.2	0.11	321	269	0.86	149	2782 ± 18	2788 ± 12	2794 ± 36
7.1	–	118	53	0.47	51.5	2655 ± 32	2719 ± 19	2848 ± 83
7.2	0.14	316	104	0.34	148	2807 ± 18	2773 ± 16	2751 ± 63
8.1	0.46	328	37	0.12	105	2039 ± 15	2247 ± 21	2210 ± 180
8.2	0.10	357	123	0.36	163	2744 ± 16	2785 ± 11	2762 ± 57
171/1, metagraywacke								
1.1	0.20	243	297	1.26	107	2658 ± 21	2778 ± 15	2602 ± 39
1.3	0.18	190	125	0.68	80.2	2572 ± 24	2737 ± 17	2636 ± 56
2.1	0.13	134	117	0.90	59.6	2679 ± 28	2743 ± 20	2638 ± 59
2.2	0.07	148	107	0.75	67.6	2746 ± 28	2771 ± 18	2752 ± 68
9.1	0.56	173	98	0.58	81.4	2798 ± 29	2757 ± 19	2609 ± 77
10.1	0.90	57	28	0.51	25.8	2715 ± 45	2799 ± 39	2667 ± 190
3.1	0.22	156	104	0.69	73.8	2827 ± 27	2760 ± 19	2767 ± 70
4.1	0.59	82	85	1.07	36.1	2668 ± 40	2735 ± 31	2583 ± 88
4.2	0.21	48	26	0.56	20.6	2607 ± 45	2759 ± 35	2659 ± 130
1253/2, andesite metatuff								
Core								
1.1	0.04	84	65	0.80	37.7	2699 ± 35	2722 ± 24	2842 ± 83
2.1	0.00	133	85	0.66	62.3	2801 ± 44	2735 ± 18	2841 ± 74

Table 3. (Contd.)

Point	% $^{206}Pb_c$	ppm U	ppm Th	$^{232}Th/^{238}U$	ppm $^{206}Pb*$	(1) $^{206}Pb/^{238}U$ age	(1) $^{207}Pb/^{206}Pb$ age	(1) $^{208}Pb/^{232}Th$ age
2.2	0.43	22	8	0.39	9.47	2596 ± 67	2725 ± 64	2829 ± 380
2.3	–	115	64	0.57	50.7	2673 ± 30	2713 ± 20	2775 ± 76
3.1	0.36	54	24	0.45	26	2873 ± 46	2806 ± 35	2893 ± 200
4.1	–	104	82	0.82	41	2445 ± 29	2596 ± 24	2605 ± 65
5.1	0.64	48	54	1.15	22.6	2779 ± 99	2719 ± 46	2596 ± 160
6.1	0.06	165	68	0.43	73.9	2703 ± 26	2773 ± 17	2715 ± 72
7.1	0.12	442	400	0.93	200	2724 ± 19	2743 ± 11	2694 ± 35
8.1	0.07	607	4	0.01	214	2218 ± 12	2392 ± 15	2020 ± 1400
8.2	0.08	60	25	0.44	29	2890 ± 45	2751 ± 34	3147 ± 200
10.1	0.85	465	3	0.01	130	1805 ± 11	1781 ± 39	
11.1	0.78	529	10	0.02	205	2379 ± 20	2465 ± 15	13533 ± 800
11.2	0.01	806	16	0.02	351	2645 ± 12	2695 ± 8	2790 ± 200
Shell								
9.1	0.49	45	24	0.54	19.7	2631 ± 72	2809 ± 41	2745 ± 200
9.2	0.06	364	2	0	102	1817 ± 13	1855 ± 20	2970 ± 2100

Note: Errors are given at the 1σ level. Pb_c and Pb* correspond to common and radiogenic lead. The common lead correction was based on measured ^{204}Pb. Sample 1253/2 was taken from the Kichany area (Fig. 1).

and Th/U = 0.01–0.93. The oldest ages were obtained for areas with well-preserved magmatic zoning. The concordant age calculated for nine points is 2735 ± 20 Ma (Table 3, Fig. 11e). The dark shells are subdivided into three age groups (Table 3, Fig. 11e). The shell of grain 7 with U = 442 ppm and Th/U = 0.93 was

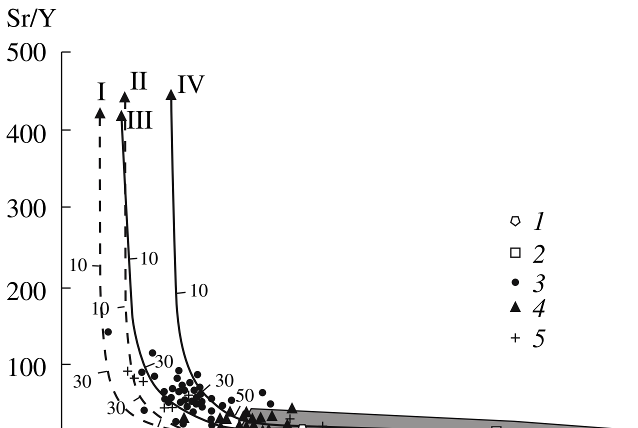

Fig. 8. Diagram Sr/Y–Y [24] for the metadacites and trondhjemites of the Kalikorva structure. (*1*) Archean mafic compositon, (*2*) MORB, (*3*) metadacite (adakite), (*4*) HREE enriched metadacite, and (*5*) trondhjemite. Curves show different models of the formation of aluminous tonalite–trondhjemite–dacite (TTD) by partial melting of an Archean mafic source (I, with eclogite or II, 10% garnet amphibolite in the residue) and MORB (III, with eclogite or IV, 10% garnet amphibolite in the residue). The percentage of partial melting is shown in each model curve. The shaded field shows low-Al island arc andesite–dacite–rhyolite (ADR) formed by crystal fractionation.

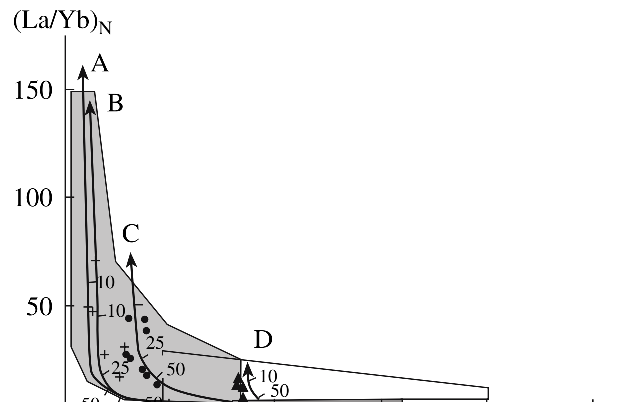

Fig. 9. Diagram Yb_N–$(La/Yb)_N$ [24] for the metadacites and trondhjemites of the Kalikorva structure. The gray field is high-Al tonalite–trondhjemite–dacite (TTD), the unfilled field is post-Archean granitoids, and the dark gray field is MORB. Letters denote model curves for the partial melting of a mafic source: A, with eclogite; B, with 25% garnet amphibolite; C, with 10% garnet amphibolite; and D, with garnet-free amphibolite in the residue. The percentage of partial melting is shown for each model curve. Other symbols are the same as in Fig. 8.

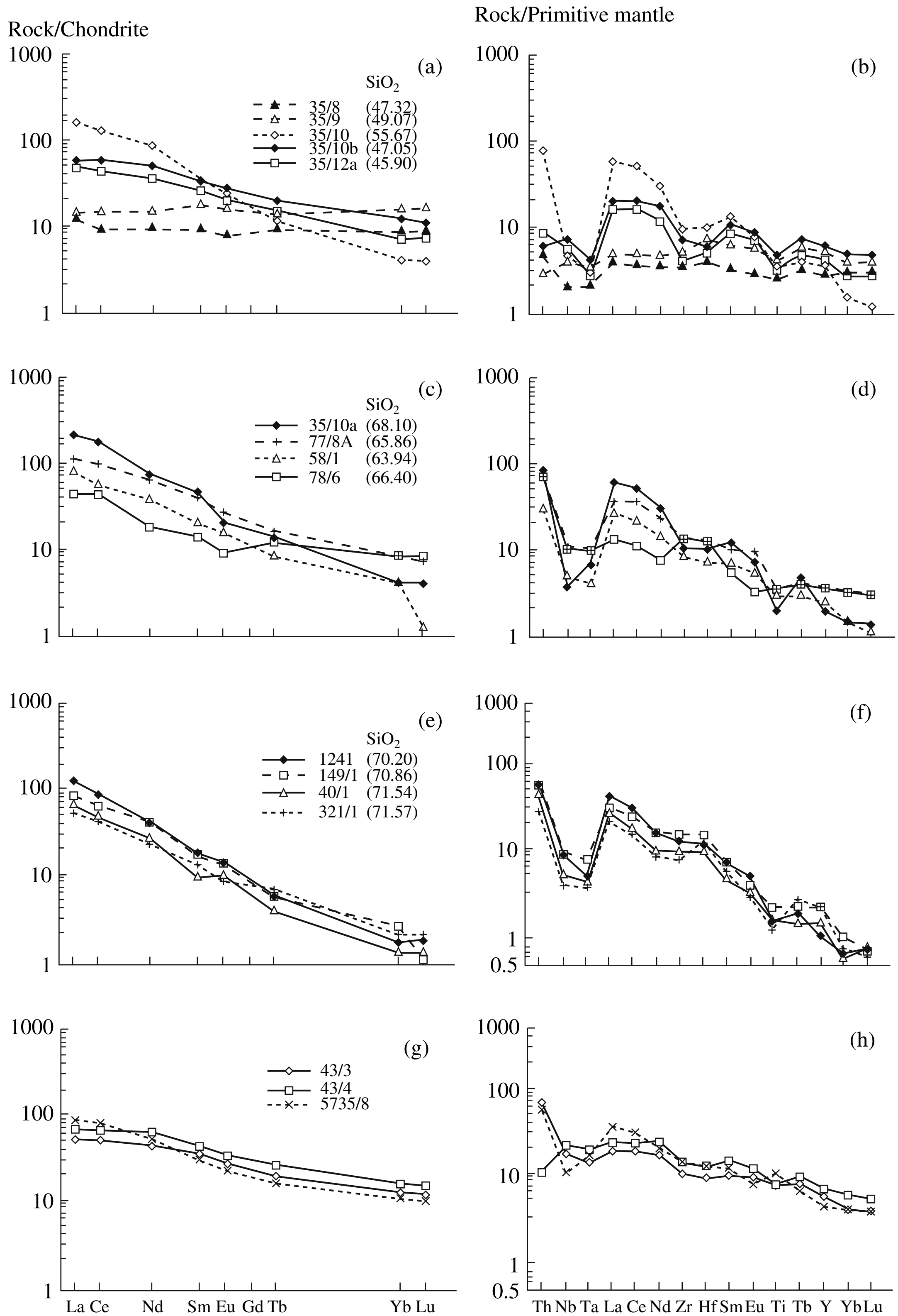

Fig. 10. Chondrite- and primitive-mantle normalized [21] REE and trace element distribution patterns for the rocks of the upper sequence of the Kalikorva structure. (a, b) Ultramafic and mafic rocks. (c, d) Metadacites. (e, f) Trondhjemites. (g, h) Fe metabasalts. Sample numbers correspond to those of chemical analyses in Table 2.

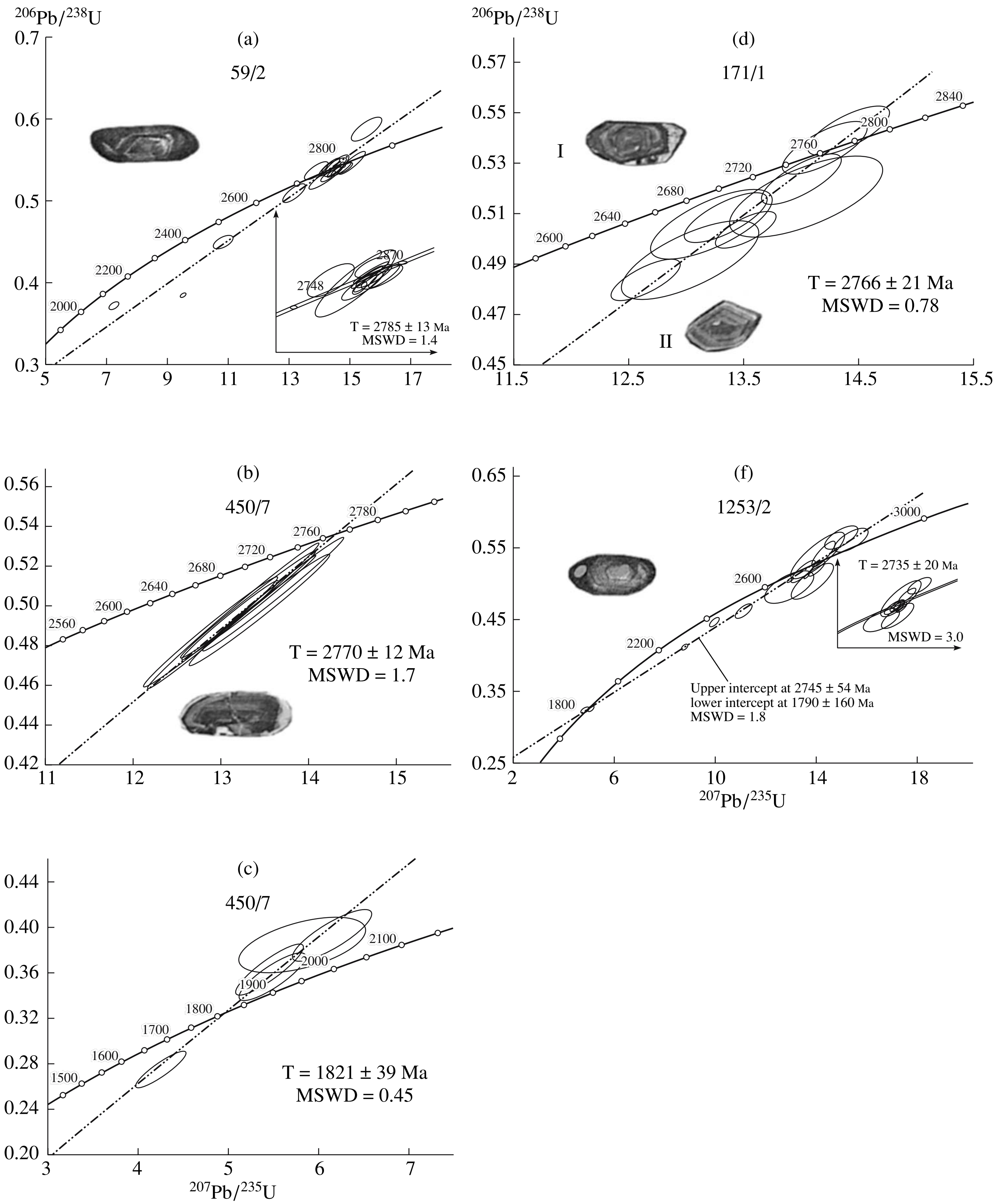

Fig. 11. Concordia diagram for zircons. Sample numbers correspond to those of chemical analyses in Tables 1 and 2. Sample 1253/2 is andesite metatuff from the volcanic section of the Tikshozero greenstone belt, Kichany area. Also shown are the cathodoluminescent images of zircons.

Table 4. Sm–Nd isotopic data for the rocks of the Belomorian belt

Sample No.	U-Pb age	Sm ppm	Nd ppm	$^{147}Sm/^{144}Nd$	$^{143}Nd/^{144}Nd$ ($\pm 2\ \sigma_{meas}$)	$\varepsilon_{Nd}(0)$	$\varepsilon_{Nd}(T)$	$T_{Nd}(DM)$	$T_{Nd}(DM\text{-}2st)$
Supracrustal sequences									
Pulonga area [13]									
4655/5	2870	2.834	17.13	0.1000	0.510989	–32.2	3.6	2883	2890
Kalikorva area [13]									
59/2	2785	3.769	26.69	0.0853	0.510771	–36.4	3.5	2811	2821
77/1	2785	4.487	25.43	0.1066	0.511121	–29.6	2.7	2875	2887
444/3	2770	3.287	19.86	0.1000	0.510978	–32.4	2.1	2897	2924
445/5a	2770	4.010	23.94	0.1003	0.511004	–31.9	2.5	2870	2894
Kichany area [8]									
451/2	2720	4.390	25.45	0.1044	0.510921	–33.5	–1.2	3091	3153
1005a	2735	4.830	26.91	0.1085	0.510991	–32.1	–1.1	3111	3157
1016b	2735	5.210	26.07	0.1207	0.511312	–25.9	0.9	2997	2995
Tonalites from the southwestern part of Lake Kovdozero [11]									
321/1	2785	2.120	11.59	0.1098	0.511114	–29.7	1.4	2972	2992
325/1	2785	1.400	11.97	0.0701	0.510442	–42.8	2.6	2860	2899
341/1	2785	7.663	51.37	0.0895	0.510771	–36.4	2.0	2905	2944
350/1	2785	1.870	10.87	0.1031	0.511066	–30.7	2.9	2858	2871
1233	2785	1.774	13.95	0.0762	0.510545	–40.8	2.4	2873	2914
1244	2785	5.470	31.80	0.1030	0.511041	–31.2	2.5	2890	2909

Note: Rocks: 4655/5, 59/2, 77/1, 444/3, and 445/5a are metadacites; 451/2 is metaandesite–dacite tuff; 1005a is metaandesite–dacite; and 1016b is metaandesite.

probably formed during the late magmatic stage. The age of metamorphism calculated from the lower intercept of 16-point discordia is 1790 ± 160 Ma, and a more accurate concordant age of 1796 ± 40 Ma was obtained for the shells of grains 9 and 10 (U = 364–465 ppm and Th/U = 0.01) (Fig. 11e).

DISCUSSION AND CONCLUSIONS

The lower sequence of the Kalikorva structure is dominated by metatholeiites with high contents of MgO, Cr, and Ni, high *Mg*# and REE contents close to the mantle level. They contain rare interlayers of komatiites and lenses of pyroxenites and peridotites and could be considered as products of the deep melting of mantle material. At the same time, tholeiite metabasalts have island-arc signatures and are intercalated with metagraywackes and metadacites (adakites), the magmas of which were generated in the zone of oceanic slab subduction beneath the continental plate [24]. This rock association could be formed in a spreading environment at the beginning of the island-arc stage [32].

The upper sequence is dominated by metagraywackes and contains diverse magmatic rocks with MORB (tholeiitic and komatiitic basalts) and island-arc characteristics (calc-alkaline dacites and andesites, subalkaline basalts, and picritic basalts). Such a diversity of magmatic rocks is observed in back-arc basins [27].

The association of dacites (adakites) with Nb-enriched Fe–Ti basalts and basaltic andesites is indicative of a subduction regime. Similar associations occur in Cenozoic arcs [33] and were recently found in some Late Archean (2.7 Ga) greenstone belts of the Superior Province, Canada, for example, in Wawa [34] and Uchi [26, 27]. The presence of HREE-enriched dacites, which could be formed by fractional crystallization, as well as mafic–ultramafic subalkaline rocks marks a transition to a more mature stage of island arc evolution.

The U–Pb ages of zircons from the metadacites and detrital zircons from the metagraywackes of the Kalikorva structure are similar and range from 2785 ± 13 Ma to 2766 ± 21 Ma. They coincide with an age of 2780 Ma obtained for the late volcanic complex of the Hisovaara Group of the Hisovaara structure [9]. Both complexes include island arc associations with subduction signatures, and contain adakites, Nb–Ti basalts, and basaltic andesites.

A similar volcanic association was previously studied by us in the Kichany and Zarechensk areas in the Tikshozero greenstone belt [8]. However, the age of

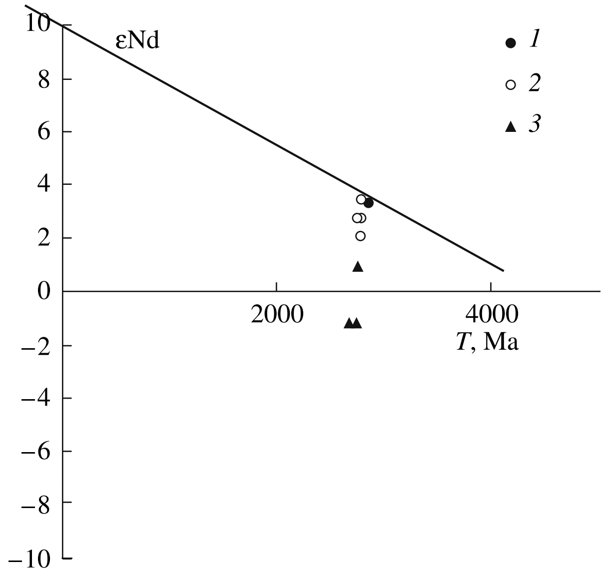

Fig. 12. Diagram εNd–T [37] for metavolcanic rocks from the structures located at the junction of the Karelian craton with the BMB. The samples of felsic metavolcanics (Table 4) were taken from (*1*) the Chupa nappe (sample 4655/5), (*2*) the Kalikorva structure (samples 59/2, 77/1, 444/3, and 445/5a), and (*3*) the Tikshozero greenstone belt, Kichany area (samples 451/2, 1005a, and 1016b).

metaandesites from the middle sequences of the Kichany area (sample 1253/2, Table 3) is 2735 ± 20 Ma and younger than the age of the Kalikorva rocks. A U–Pb zircon age of 2720 ± 4 Ma was obtained for metaandesites from the upper sequence [35]. The volcanic complex of the Kichany area probably represents a younger island arc.

The metadacites and metgraywackes of the Chupa sequence [36] are older than similar rocks of the Kalikorva Complex. This fact, together with the geochemical features of the rocks and geodynamic conditions of their formation (back-arc basins), indicates that the Kalikorva Complex could not be part of the Chupa nappe underthrust beneath the margin of the Karelian craton but is a fragment of the Tikshozero greenstone belt, which is identified as an island-arc system.

The previously published Sm–Nd data [8, 11, 13] for the supracrustal rocks that compose the transitional zone between the Belomorian mobile belt (BMB) and the Karelian craton and the obtained U–Pb ages allowed us to draw the following conclusions.

Given the large uncertainty of calculations, the supracrustal rocks of all the structures (Pulonga, Kalikorva, and Kichany areas) have similar Sm–Nd model ages. They fall within the following intervals (from west to east): 2880–2910 Ma for the Chupa sequence, Pulonga area, 2860–2923 Ma for the Kalikorva area, and 2800–3111 Ma for the Kichany area (Table 4). The protolith of the tonalite–trondhjemite association was emplaced later (also relative to the formation of at least the oldest volcanic rocks) in the junction zone of the Karelian craton with the Belomorian mobile belt [11]. This indicates an almost simultaneous melt segregation from the mantle reservoir over the territory spanning the aforementioned structures. There is only some tendency of a westward increase in the age of initial crust formation. However, similar U–Pb and Sm–Nd ages were obtained only for the Chupa sequence (Pulonga area) [13, 36], which indicate an uncontaminated mantle source of these melts. In all other rocks, U–Pb ages are younger than model Sm–Nd ages, which is expressed in variations in εNd values (Table 4). This parameter decreases westward, acquiring negative values in the rocks of the Kichany area (Fig. 12). The change of εNd from positive values corresponding to the depleted mantle in the BMB (Pulonga area) to negative values in the western structures (Kichany area) may indicate a gradual dilution of the mantle source by crustal material owing to the proximity of the craton.

ACKNOWLEDGMENTS

This study was supported by the Federal Programs for the Support of Leading Scientific Schools, project no. NSh-615.2003.5.

REFERENCES

1. Yu. V. Miller and R. I. Mil'kevich, "Fold-and-Thrust Structure of the Belomorian Tectonic Zone and Its Relations with the Karelian Granite–Greenstone Terrane," Geotektonika, No. 6, 80–92 (1995).
2. V. A. Glebovitskii, Yu. V. Miller, G. M. Drugova, et al., "The Structure and Metamorphism of the Belomoride–Lapland Collision Zone," Geotektonika, No. 1, 63–75 (1996) [Geotectonics **30**, 53–63 (1996)].
3. Yu. V. Miller, T. A. Myskova, and R. I. Mil'kevich, "Supracrustal Rocks in the Tectonic Windows of the Marginal Part of the Karelian Craton (Northwestern Belomorian Province)," Geotektonika, No. 1, 13–28 (2002) [Geotectonics **36**, 11–23 (2002)].
4. *Early Precambrian of the Baltic Shield*, Ed. by V. A. Glebovitskii (Nauka, St. Petersburg, 2004) [in Russian].
5. A. I. Slabunov, "Late Archean Active Continental Margin of the Karelian Plate, Baltic Shield," in *Proceedings of International Conference on the Precambrian of Northern Eurasia* (IGGD RAN, St. Petersburg, 1997), p. 95 [in Russian].
6. V. N. Kozhevnikov, *Archean Greenstone Belts of the Karelian Craton as Accretionary Orogens* (Kar. NTs RAN, Petrozavodsk, 2000) [in Russian].
7. A. A. Shchipansky, I. I. Babarina, K. A. Krylov, et al., "The Oldest Ophiolites: The Late Archean Suprasubduction Zone Complex of the Iringora Structure, North Karelian Greenstone Belt," Dokl. Akad. Nauk **377**, 376–380 (2001) [Dokl. Earth Sci. **377**, 283–287 (2001)].
8. R. I. Mil'kevich, Yu. V. Miller, V. A. Glebovitskii, et al., "Tholeiitic and Calc-Alkaline Magmatism in the Northern Part of the Tikshozero Greenstone Belt: Geochemical Evidence of a Subduction Environment,"

Geokhimiya, No. 12, 1262–1274 (2003) [Geochem. Int. **41**, 1152–1164 (2003)].

9. E. V. Bibikova, A. V. Samsonov, A. A. Shchipanskii, et al., "The Hisovaara Structure in the Northern Karelian Greenstone Belt as a Late Archean Accreted Island Arc: Isotopic Geochronological and Petrological Evidence," Petrologiya **11**, 289–320 (2003) [Petrology **11**, 261–290 (2003)].
10. Yu. V. Miller, V. A. Glebovitskii, T. A. Myskova, et al., "Composition, Structural Setting, and Geotectonic Implications of the Chupa Nappe in the White Sea Mobile Belt: New Data," Dokl. Akad. Nauk **366**, 379–382 (1999) [Dokl. Earth Sci. **366**, 486–489 (1999)].
11. Yu. V. Miller, A. B. L'vov, T. A. Myskova, et al., "Search for Ancient Continental Crust at the Junction of the Karelian Craton–Belomorian Mobile Belt: Evidence from Isotope Geochemistry," Dokl. Akad. Nauk **389**, 345–348 (2003) [Dokl. Earth Sci. **389**, 302–305 (2003)].
12. N. V. Gorlov, *Structure of Belomorides* (Nauka, Leningrad, 1967) [in Russian].
13. T. A. Myskova, V. A. Glebovitskii, Yu. V. Miller, et al., "Supracrustal Sequences of the Belomorian Mobile Belt: Protoliths, Age, and Origin," Stratigr. Geol. Korrelyatsiya, No. 6, 3–19 (2003) [Stratigr. Geol. Correlation **11**, 535–549 (2003)].
14. M. J. Le Bas, R. W. Maitre, A. Streckeisen, and A. Zanetin, "A Chemical Classification of Volcanic Rocks Based on the Total Alkali–Silica Diagram," J. Petrol. **27**, 745–750 (1986).
15. L. S. Jensen, "A New Cation Plot for Classifying Subalkalic Volcanic Roks," Ontario Dept. Mines **66**, (1976).
16. K. C. Condie, *Archean Greenstone Belts* (Elsevier, Amsterdam, 1981; Mir, Moscow, 1983).
17. *Early Precambrian Komatiites and Highly Magnesian Volcanics of the Baltic Shield* (Nauka, Leningrad, 1988) [in Russian].
18. A. C. Kerr, R. V. White, and A. D. Saunders, "LIP Reading: Recognizing Oceanic Plateaux in the Geological Record," J. Petrol. **41**, 1041-1056 (2000).
19. R. Kerrich, A. Polat, D. Wyman, and P. Hollings, "Trace Element Systematics of Mg- to Fe-Tholeiitic Basalt Suites of the Superior Province: Implications for Archaean Mantle Reservoirs and Greenstone Belt Genesis," Lithos. **46**, 163–187 (1999).
20. A. V. Stepanova, A. N. Larionov, E. V. Bibikova, et al., "Early Proterozoic (2.1 Ga) Fe-Tholeiitic Magmatism of the Belomorian Province, Baltic Shield: Geochemistry and Geochronology," Dokl. Akad. Nauk **390**, 528–532 (2003) [Dokl. Earth Sci. **390**, 607–610 (2003)].
21. S. S. Sun and W. F. McDonough, "Chemical and Isotopic Systematics of Oceanic Basalts: Implications for Mantle Composition and Processes," in *Magmatism in the Ocean Basins*, Spec. Publ. Geol. Soc. London **42**, 313–345 (1989).
22. H. Martin, "Adakitic Magmas: Modern Analogues of Archaean Granitoids," Lithos. **46**, 411–429 (1999).
23. A. V. Samsonov, Doctoral Dissertation in Geology and Mineralogy (Moscow, 2004).
24. M. S. Drummond and M. J. Defant, "A Model for Trondhjemite–Tonalite–Dacite Genesis and Crustal Growth Via Slab Melting: Archaean To Modern Comparisons," J. Geophys. Res. **95**, 503–521 (1990).
25. S. B. Lobach-Zhuchenko, N. A. Arestova, V. P. Chekulaev, et al., "Geochemistry and Petrology of 2.40–2.45 Ga Magmatic Rocks in the North-Western Belomorian Belt, Fennoscandian Shield, Russia," Precambrian Res. **92**, 223–250 (1998).
26. P. Holling and R. Kerrich, "An Archaean Arc Basalt–Nb–Enriched Basalt–Adakite Association: The 2.7 Ga Confederation Assemblage of the Birch-Uchi Greenstone Belt, Superior Province," Contrib. Mineral. Petrol. **139**, 208–226 (2000).
27. P. Hollings, G. Stott, and D. Wyman, "Trace Element Geochemistry of the Meen-Dempster Greenstone Belt, Uchi Subprovince, Superior Province, Canada: Back-Arc Development on the Margins of an Archaean Protocontinent," Can. J. Earth Sci. **37**, 1021–1038 (2000).
28. L. P. Black, S. L. Kamo, C. M. Allen, et al., "TEMORA 1: A New Zircon Standard for U–Pb Geochronology," Chem. Geol. **200**, 155–170 (2003).
29. K. P. Ludwig, "SQUID 1.00. A User's Manual," Berkley Geochronol. Center Spec. Publ., No. 2 (2000).
30. I. S. Williams, "U–Pb–Th geochronology by ion microprobe," in *Applications of Microanalytical Techniques to Understanding Mineralizing Processes*, Ed. by M. A. McKibben, W. C. Shanks III, and W. I. Ridley, Rev. Econ. Geol. **7**, 1–35 (1998).
31. L. P. Black, S. L. Kamo, and C. M. Allen, et al., Chem. Geol. **200**, 155–170 (2003).
32. J. L. Karsten, E. M. Klein, and S. B. Sherman, "Subduction Zone Geochemical Signature in Ocean Ridge Basalts from the Southern Chile Ridge: Implications of Modern Ridge Subduction Systems for Archaean," Lithos. **37**, 143–161 (1996).
33. M. S. Drummond, M. J. Defant, and P. K. Kepezhinskas, "Petrogenesis of Slab-Derived Trondhjemite–Tonalite–Dacite/Adakite Magmas," Trans. R. Soc. Edinburgh Earth Sci. **87**, 205–215 (1996).
34. A. Polat and R. Kerrich, "Magnesian Andesites, Nb-Enriched Basalt-Andesites, and Adakites from Late-Archaean 2.7 Ga Wawa Greenstone Belts, Superior Province, Canada: Implication for Late Archaean Subduction Zone Petrogenetic Processes," Contrib. Mineral. Petrol. **141**, 36–52 (2000).
35. O. A. Levchenkov, R. I. Mil'kevich, Yu. V. Miller, et al., "U–Pb Isotope Age of Metaandesites in the Upper Sequence of the Tikshozero Greenstone Belt Northern Karelia)," Dokl. Akad. Nauk **389**, 378–381 (2003) [Dokl. Earth Sci. **389**, 384–387 (2003)].
36. E. V. Bibikova, V. A. Glebovitskii, S. Claesson, et al., "New Isotopic Data on the Protolith Age and Evolutionary Stages of the Chupa Formation, Belomorian Belt," Geochem. Int. **39** (Suppl. 1), 512–517 (2001).
37. S. B. Jacobsen and G. J. Wasserburg, "Sm–Nd Evolution of Chondrites and Achondrites," Earth Planet. Sci. Lett. **67**, 137–150 (1984).